



Temperatures of impervious surfaces in rural Montana

David Carlson¹

¹ retired. Near Bozeman Montana, USA

Correspondence to: David Carlson (ipy.djc@gmail.com)

5 **Abstract.** Data described here demonstrate utility of bicycles as platforms for and carriers of modern small capable sensors. For two years (September 2021 to October 2023), I rode a bicycle carrying sensors that simultaneously measured GPS time and position, air temperature(s), surface temperature, downwelling visible and UV light, spectrally-resolved upwelling (reflected) light, plus air flow. I rode more than 170 times, covering a standard 15 km rural loop or along ~12 km paths to and from Bozeman, over a range of times and weather. To accommodate frequent snow and ice conditions, I walked the
10 same bike carrying the same sensors more than 30 times back and forth along a quiet stretch of paved (mostly) snow-covered surface. Because loop and to/from Bozeman routes ran along an identical 3 km stretch of rural highway, that stretch represents one of the most-measured extents of impervious surface. Routes covered impervious paved surfaces punctuated by intervals of gravel or tree-shade or both. Sensors, adopted from consumer applications, produced reliable repeatable data. I achieved spatial resolutions of 4 to 5 meters and temperature resolutions of 0.5oC; a typical ride of 45 minutes produced
15 ~4000 clean data records. These data serve a wide variety of engineers and scientists exploring pavement temperatures, heat islands, surface run-off, etc. Users can access all data following guidance as follows:

Time period	DOI	Image file DOI	Reference
Summer 2022-2023 (71 rides)	https://doi.org/10.5281/zenodo.15053252	https://doi.org/10.5281/zenodo.15053336	Carlson 2025b
Fall 2021-2023 (54 rides)	https://doi.org/10.5281/zenodo.15053261	https://doi.org/10.5281/zenodo.15053390	Carlson 2025c
Miscellaneous (53 files)	Sensor sheets, source files, pictures, etc.	https://doi.org/10.5281/zenodo.15054004	Carlson 2025d

A set of screenshot images of combined sensor data time series, recorded for every ride, exists at separate Zenodo addresses; see table above and Data Description below. Users can familiarize themselves with these data by viewing a short (<5 minute)
20 proof-of-concept video available at <https://youtu.be/nMjBFbXxNWU>.



1 Introduction

Note: As a private citizen this author has no access to, nor intent nor capacity to purchase access to, paywalled, proprietary or otherwise protected information. Reviewers or authors of related manuscripts must accept these omissions; unless abstract contained useful information, I made neither use nor mention of non-open access publications.

- 25 Impervious surfaces, ranging from local streets and parking lots to cross-country highways and airport runways, facilitate movements of people and goods. One can identify benefit (easy rapid transport) and general convenience but also ham (altered run-off of surface water and changed absorption of solar radiation relative to vegetation). Frequently constructed over large areas, impervious surfaces - whether occupied by vehicles or empty - affect diel, seasonal and annual thermal and hydrological properties.
- 30 Unfortunately, many remote sensing techniques struggle to keep pace with expansions of impervious surfaces (He et al. 2023, Zhang et al. 2022) and lack spatial resolution or optical discrimination to distinguish urban from rural settings or shaded from unshaded surfaces. While different regions experience distinct development patterns, roads (paved impervious routes constructed primarily for motorized vehicle transit) constitute expanding components of most urban developments and play disproportionate roles in heat island effects (e.g., Ibrahim et al. 2016).
- 35 How then should researchers map impervious surfaces and local roads or paths to assess heating or run-off impacts or to confirm outcomes of algorithmic analyses of remotely-sensed information? In particular, what measurements over what surfaces might serve as necessary baselines for urban heat island studies? Does solar heating of impervious surfaces, which then in turn modify thermal properties of overlying air (e.g., as outlined by Pomerantz et al. 2000), pertain in rural settings? If not, what do these data show about heat island effects and what additional factors must researchers explore?
- 40 Many weather services maintain sensor systems in protected locations away from development, for reliable long-term measurements of temperature, humidity and wind; they avoid nearby impervious surfaces so as to not impact essential measurements by adjacent surface heating. At the same time, however, researchers need improved measurements of heating and run-off patterns over paved surfaces, particularly as larger portions of global populations reside in urban settings containing substantial areas of impervious surfaces. How will observation communities validate remote sensing at spatial
- 45 resolutions of 30 meter or better (Zhang et al. 2020) if local resolution remains insufficient to distinguish paved impervious from unpaved pervious surfaces?

- Bicycles represent one under-used solution. Bicycles impose few or no heat inputs and minimal flow distortion. Bicycles can travel along or across roads and other impervious surfaces, often as those routes pass through building- or tree-induced shade or connect to graveled, grassy or other pervious or impervious paths. Bicycles can carry lightweight accurate low-power
- 50 sensors of extraordinary capability and variety. A fleet of bicycles carrying inexpensive reliable sensor packages could repeatedly explore and document surface types and temperatures typical of many cities, as key partners in understanding and mediating heating and run-off impacts. Bicycles have served as platforms for measurements, albeit in awkward attempts to duplicate 'standard' meteorological instrumentation (e.g., Samad & Vogt 2016), generally over short times to cover extreme (warm) conditions (e.g., Raikovich & Larson 2016, Lehnert et al 2018), rarely including both air and surface temperature



55 measurements (e.g., Brandsma & Wolters 2012, Kousis et al. 2021) nor a larger-range of sensors as described here and -
unfortunately but consistently - without sharing data.

Here I describe data from a standard bicycle carrying a small low-cost highly-reliable sensor package, deployed more than
200 times over two years. Sections 2 and 3 briefly describe Montana travel surfaces and the particular bicycle. Section 4
addresses sensor types and deployment. Section 5 describes data collected over two years from a variety of paved and gravel,
60 full-sun and tree-shaded, and warm and cold surfaces, with appropriate validations and examples. Section 6 addresses
validation and uncertainties not addressed in previous sections. Section 7 considers implications of these data specifically
and of bicycle-gathered data generally.

A data description section (Section 8) describes exact formats of data, images and availability of useful accessory data; see
table above. Users might first view a short video (<https://youtu.be/nMjBFbXxNWU>) to familiarize themselves with bicycle-
65 based measurements, modern sensors, and issues related to mobile measurements at high spatial resolutions. Section 9 offers
summary assessments and a hopeful look forward.

2 Local environments of these data

While many areas surrounding the central node of Bozeman Montana undergo rapid urbanization, these particular data
derive from a region that, during these measurements, qualified as ‘sparsely built’ (Demuzere et al. 2022). Figure 1
70 demonstrates: measurements along a repeated 15-km local route (Fowler loop, always - with one exception - ridden
clockwise); bicycle-based data collection over routes to and from Bozeman proper (Bozeman, ~12 km each way), passing
through sparsely built to ‘open midrise’ environments (Demuzere et al. 2022) via a series of paved roads (~60%)
interconnected by bicycle-friendly pedestrian-focused paths (~40%); and walking measurements, using same sensors and
bicycle, over a 0.25 km stretch of rural pavement initially snow-covered then gradually exposed as melting occurred (Fig. 1
75 inset). Data from Fowler loop and Bozeman routes coincided along a ~3 km north-south stretch of sun-warmed nearly-
treeless pavement on south 3rd Avenue (evident in Fig. 1). In total I used this bicycle to record reliable data from 171 rides
and 31 walks over 25 months covering a range of diel, seasonal and weather conditions.

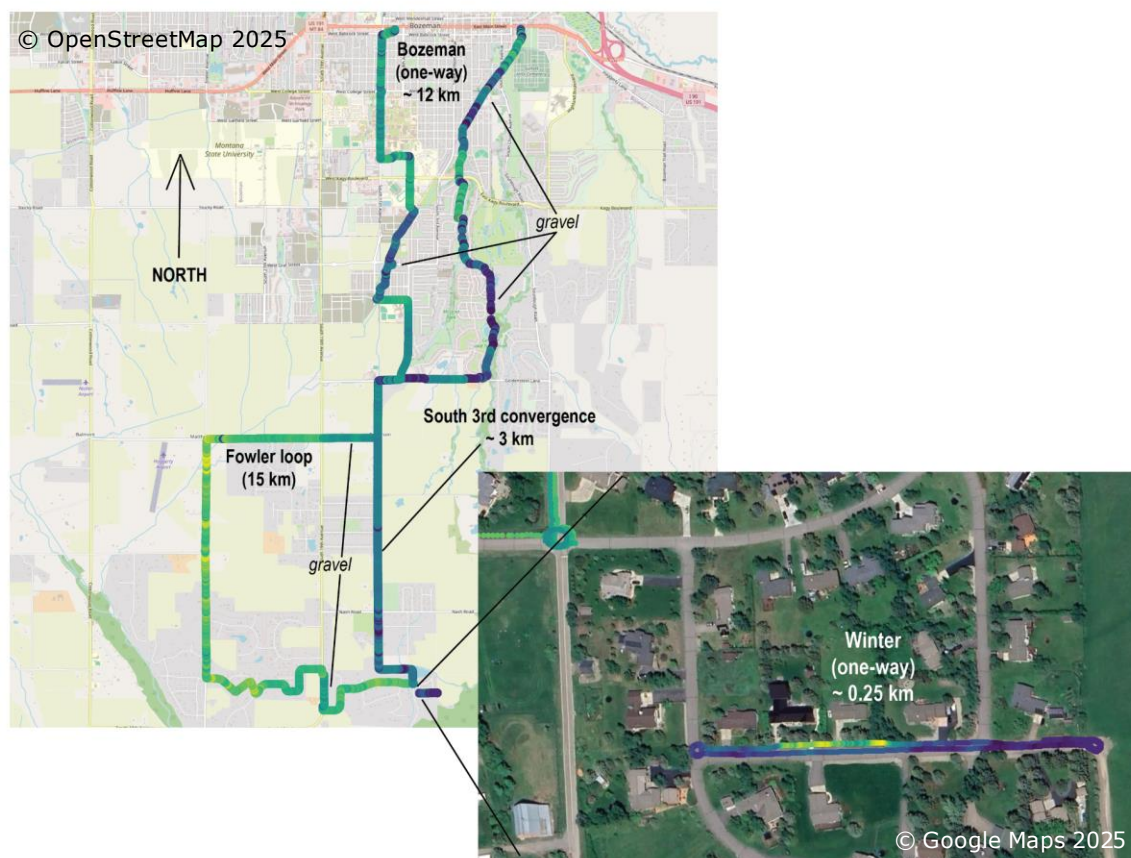
Pavement engineers classify these surfaces as ‘chip-sealed’: mixtures of asphalt binding materials with small stone
inclusions. In rare spots, original darker asphalt (with fewer stone inclusions) had not yet received particle-rich chip-seal top
80 coats. Pavement colors, dominated by inclusions of local stones, varied only slightly: gray to darker gray. I rarely rode over
whiter concrete surfaces, generally only at recently-constructed intersections or freshly-paved surfaces in downtown
Bozeman.

Data presented here came primarily from local county (Gallatin) or urban (Bozeman) roads; for the most part they qualify -
by width, boundaries and surface and subsurface preparation - as ‘local roads and streets’ under State of Montana definitions
85 (State of Montana Pavement Design Manual, available at <https://mdt.mt.gov/publications/manuals.aspx>). As for other states,
the State of Montana follows US federal pavement guidelines and disseminates materials largely to guide pavement
contractors; pavement manuals focus primarily on durability. A pavement engineer might consider asphalt-based chip-sealed



90

surfaces as ‘flexible’ while regarding concrete surfaces as ‘inflexible’; this data set considers all pavements as impervious from hydrological and thermal perspectives, in contrast to pervious conditions encountered when traversing gravel or grasslands.



95

Figure 1: Routes of bicycle measurements of surface properties around clockwise Fowler loop or to-and-from Bozeman Montana. Routes conveyed in this case via GPS-located measurements of surface temperatures minus air temperatures, with individual records appearing continuous on these scales, against an Open Street Map background. Inset shows, at higher resolution against Google Earth background, winter walk data along Jade Street plus typical bicycle loops performed at starts and ends of Fowler loop or Bozeman rides (for further information check Fig. 4); this inset image demonstrates occasional slight mis-registration of GPS data or Google Earth imagery. Fowler loop data from 7 July 2023. Winter walk data from 16 February 2023. North and south-bound Bozeman data from 6 September 2023. Screenshots of data processed in freely-available QGIS software, with background toggles.

100

Standard 15 km (‘Fowler loop’) rides (Fig. 1) included 0.4 km of north-south gravel (‘frontage’) road (bounded before and after by N-S paved surfaces) plus 0.7 km of east-west gravel at eastern end of Patterson Road (both marked on Fig. 1). These gravel stretches represent unpaved roads, passable but graded not more frequently than twice or thrice per year. Paths traversed on routes into and back from Bozeman proper (again, denoted in Fig. 1) included gravel (crushed rock) surfaces



105 eroded only by non-motorized use or by very rare surface water flooding plus short stretches of ‘single’ track through
surrounding grass. Winter data over snow-covered roads occurred via the same bicycle and sensors pushed at walking speeds
to and fro a long snow-covered Jade Street (occasionally labelled as Jade Lane, Fig. 1 inset).
Fowler loop included large road-side trees at the northwest corner and again at the east-west uphill ditch-crossing stretch
near the southern terminus. Tree coverage (from conifers or seasonally-varying deciduous trees) at these locations extended
110 across the roads, imposing shade at almost all hours. Other tree shadows, where present, depended strongly on sun angles;
shade extended across both lanes of north-south travel only during early morning or late afternoon hours. Each data record
includes precise location and time of day from which users can easily calculate effective sun angles and surface exposures;
Section 5.5 conveys details of tree-induced shading. Routes to-and-from Bozeman proper passed through consistently shaded
areas near or under creek-side trees. In all cases, data from sky-exposed optical sensors (visible and UV) provided good
115 records of immediate solar exposure.

3 Bicycle

I collected these data using a sensor box attached to front rack of a Surly Big Easy bicycle (Fig. 2). Despite occasional
removals of sensor box for cleaning or upgrade (particularly after mishap on 18 November 2022), location, height,
orientation and power (tapped from a USB port on the battery-powered handlebar-mounted light, Fig. 2) remained constant
120 for all deployments. The bicycle itself provided steady speeds (via electric assist) and good traction (due to large tires) over
many surfaces including gravel and snow.

I recorded times and positions from a bar-mounted Garmin cyclometer and independently from a controllable GPS in the
sensor box (shown in Figs. 2, 3 and 4). Except when rider forgot to initiate bike-mounted Garmin, GPS records coincided
perfectly in location while providing very accurate time synchronization (e.g., panel ‘b’ of Fig. 4). Most rides started with
125 intersection-wide loops to assess direction-dependence of sensor biases (see for example first or last seconds of nearly any
record). Figure 4c shows an example of sensor box (higher time resolution) and Garmin unit (lower time resolution) GPS
data during a standard start/end loop; I forced the sensor box GPS to record at 1.5 Hz while Garmin applied a proprietary
recording interval. Although sensor data screenshot records include headings easily extracted from Garmin GPS data,
Garmin data proved redundant to, and at lower spatial resolution than, independent self-recorded GPS-based time and
130 location data from the bicycle-based sensor box (e.g., Fig. 4b). Interested users can request Garmin data as supplements to u-
blox GPS data.

Data collection on Fowler loop rides (~15 km) covered approximately 45 minutes, northbound (‘to’) Bozeman rides (~10-12
km) covered ~30-35 minutes, southbound (‘from’) Bozeman rides (~12-15 km) covered ~55 minutes. Differences relate to
specific routes and to descents northbound vs ascents southbound. For Fowler loops, average conditions over 110 rides
135 indicated 15 km in 45 minutes, for an average speed of 20 km/hour. Twenty km/hour equates to ground speed of 5.6 m/s,
suggesting effective spatial resolutions of approximately 4-5 meters. A variety of wind, surface, and traffic conditions
accelerated or delayed bicycle progress and thereby inflicted modest changes to effective spatial resolution; a ‘safe’



140 conclusion indicated 4 meters as most probable along-track spatial resolution considering this bicycle, this rider and this sensor unit under these cycling conditions. Because every data record included GPS-based timestamps and positions, a long-track resolution estimated from average bicycle speeds proved approximate. Users can determine specific spatial resolutions and location of individual sensor data according to purpose. Data presented here included no averaging, interpolation or other data processing steps.



145 **Figure 2: Surly Big Easy electric assist bicycle with sensor package mounted on front rack. A fully-charged battery typically supported 80-90 km of lowest level ('Eco' mode) assist. In general, rides northbound involved slight descents, requiring little or no battery assist. Rides southbound typically involved slight ascent, ridden generally at second-level ('Tour') assist. I never exhausted battery assist capacities. Sensors sat 70 cm above ground surfaces. Sensor box derived power from USB tap on rear of headlight.**



4. Sensors

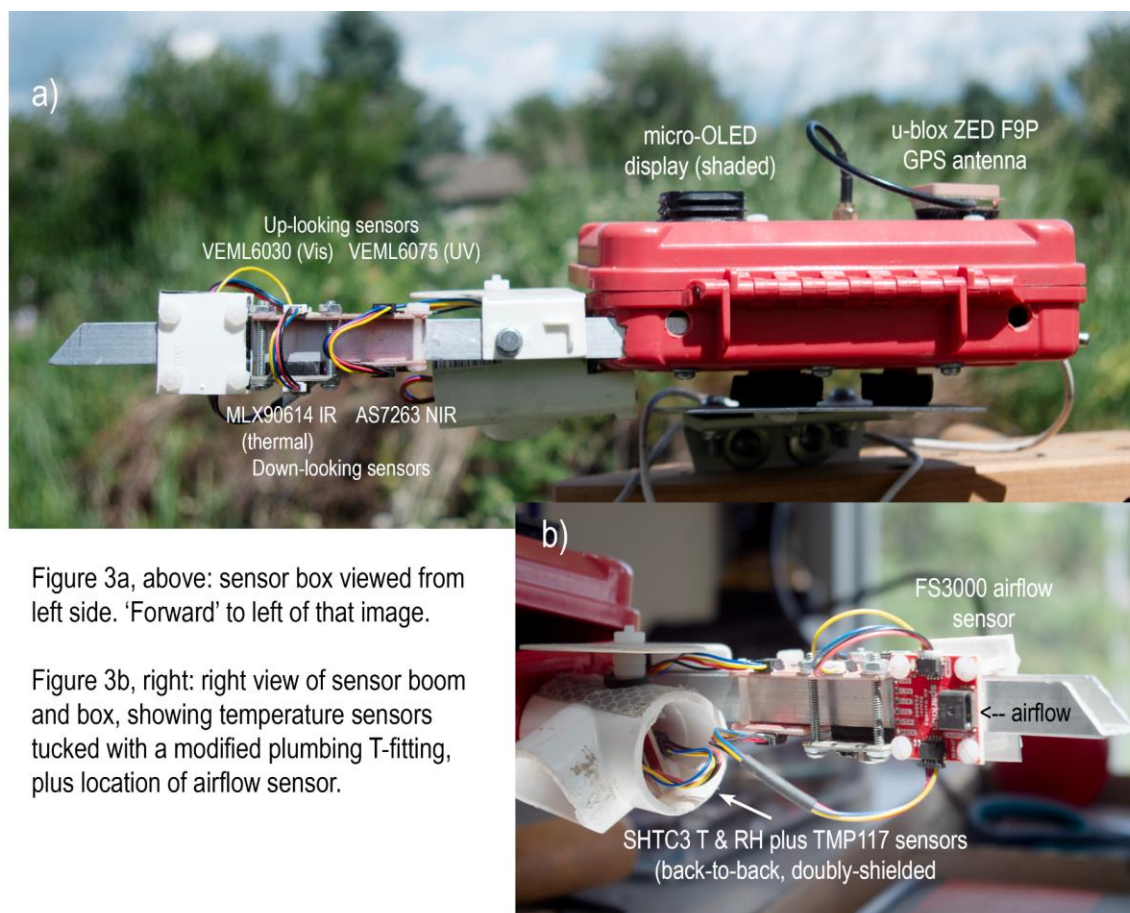


Figure 3a, above: sensor box viewed from left side. 'Forward' to left of that image.

Figure 3b, right: right view of sensor boom and box, showing temperature sensors tucked with a modified plumbing T-fitting, plus location of airflow sensor.

150

Figure 3: Sensor box showing location of all sensors from left ('a', in direction of bicycle travel) and, closer view, from right ('b'). OLED display, driven by the microcomputer, displayed three data lines including GPS time, very useful to confirm GPS synchronization and for comparison with Garmin 830 unit at start of each ride. I installed an FS3000 airflow sensor (panel b) to monitor air flows across temperature sensors. Apparent airflow-determined bike speeds (encompassing combinations of bicycle motion plus local wind speed) proved not useful for this discussion; interested users can easily compare Garmin GPS-derived bicycle speeds to FS3000 velocities from these data.

155

I operated all sensors on a single I2S bus managed by a Teensy 4.1 microcomputer. As shown in Fig. 2, sensors (up-looking, down-looking or immersed in flowing air) plus the u-blox GPS unit operated from a single box powered via a USB connection, with all sensors exposed to clean air 70 cm above ground surfaces. Up-looking sensors (Fig. 3a) included VEML6030 (visible) and VEML6075 (UV) plus the u-blox GPS antenna. Down-looking sensors (Fig. 3a) included the MLX90614 infrared (IR) surface temperature sensor plus an AS7263 near-infrared (NIR) spectral sensor. Air temperatures came from co-located doubly-shielded SHTC3 and TMP117 sensors (Fig. 3b); the SHTC3 also provided humidity data. Ahead of those sensors, in clean airflow, I operated a FS3000 air flow sensor (Fig. 3b). A much-ventilated hardware box

160



165 housed microcomputer plus u-blox GPS processing board plus a small conventional on-off switch. All sensors operated
within < 20 cm of each other: total end-to-end length for box plus boom equaled 32 cm. Total bicycle-mounted weight
including metal bracket, metal mounting plate, fasteners, bumpers, box, sensors and power and signal wires, remained under
700 g. Users could build copies of this complete sensor set for < \$300.

4.1 GPS

170 I operated a bicycle-specific Garmin 830 cyclometer in standard GPS configuration (Fig. 4a). After each ride I converted
cyclometer data via .tcx format to .csv files. For reasons of low spatial resolution and persistent redundancy, I do not include
Garmin cyclometer data with these data files; see Data Description below. To provide reference time and location data for all
sensors, and to confirm (and out-perform) cyclometer-derived location data, I operated a u-blox ZED F9P GPS as backbone
instrument of the bicycle-based sensor box (Fig. 4b & 4c). I recorded u-blox GPS time and position data along with data
from other sensors into composite .csv files.

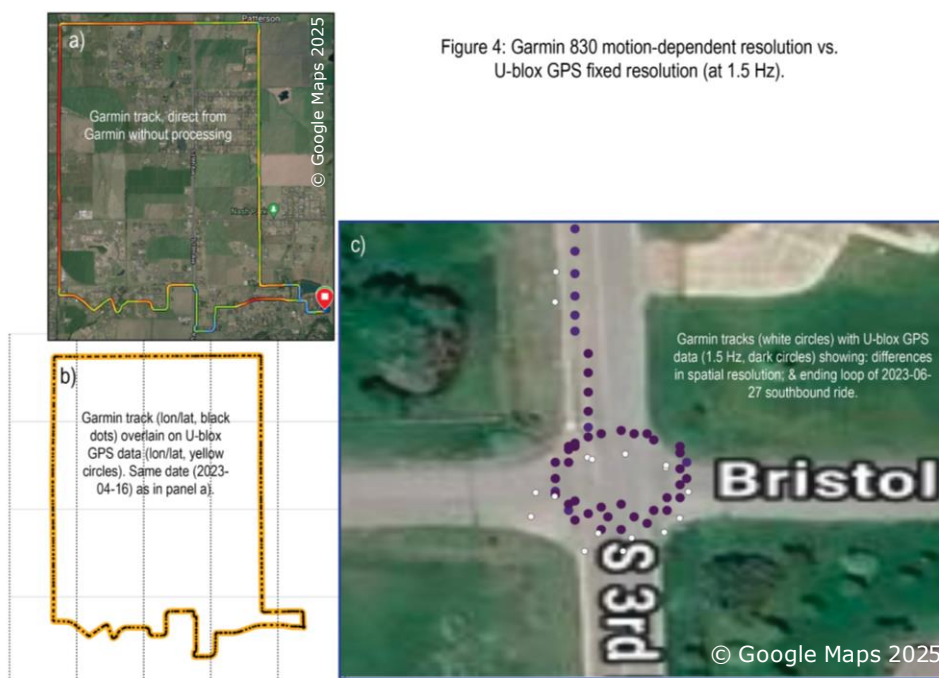


Figure 4: Garmin 830 motion-dependent resolution vs. U-blox GPS fixed resolution (at 1.5 Hz).

175
180 Figure 4: GPS data recorded on Fowler loop ride (2023-04-16) and at termination of southbound Bozeman ride (2023-06-27). Track in panel 'a' came directly from a screenshot of Garmin cyclometer data, with no processing or export. Data in panels 'b' and 'c' came from .csv files relevant to same date, with Garmin cyclometer data exported and converted via .tcx format to .csv while u-blox ZED F9P GPS location and time data (collected at fixed 1.5 Hz recording frequency) came directly from sensor box .csv files. Background in panel 'c' came from Google satellite image toggled through QGIS; slight offset occurred due to minor mis-registration of background image. Cyclometer and u-blox GPS successfully recorded lane and loop positions at better than 2 m uncertainties. All sensor data layered on user-specified backgrounds available in QGIS.



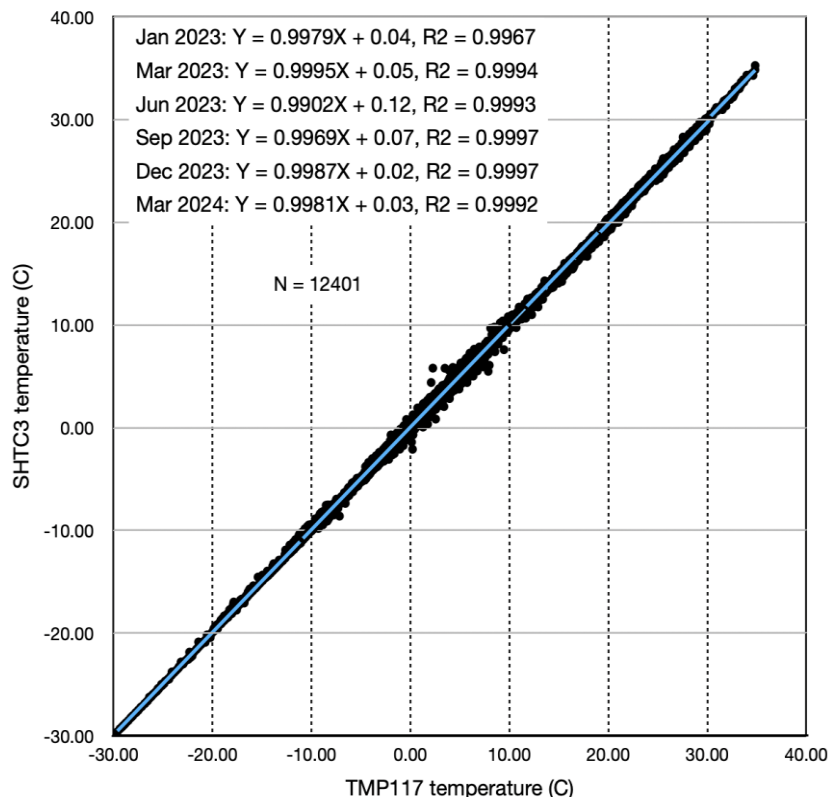
4.2 Air temperature

Until November 2022, I used a single high-resolution temperature (plus humidity) sensor, the SHTC3 unit. After November
185 2022 I added a second high-resolution TMP117 temperature sensor mounted back-to-back (< 1 cm distance) with the
SHTC3, both within a double-layer radiation-protected white-plastic (standard PVC pipe) flow-through chamber (Fig. 3b). I
purchased these (and most other) sensors mounted on Sparkfun breakout boards. Breakout boards provided onboard
processing, conversion to standard units (often oC), bus addressing systems, power conditioning, connectivity, and easy
mounting. I recorded all data from the sensor box (u-blox GPS location and time plus temperatures, humidities, visible and
190 UV light, etc.) into single per-ride .csv files. At temporal resolution of 1.5 Hz, each .csv file held ~4000 records.

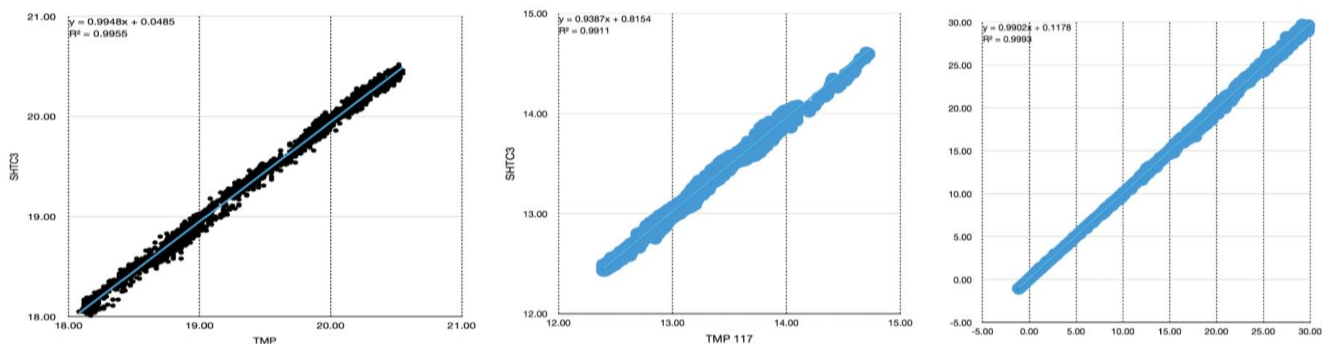
I started with a 12-bit Sensirion AG (Switzerland) SHTC3 temperature and humidity sensor. The bandgap SHTC3, intended
for consumer electronic temperature measurement applications, provided accuracy of 0.2oC over the range 0 to +60oC. I
subsequently added a 16-bit TMP117 sensor (by Texas Instruments, USA) specifying 0.1oC accuracy in the temperature
range -20 to +50oC plus documented compatibility with ASTM and ISO standards for electronic patient thermometers; it
195 functioned as a single-chip digital equivalent of a platinum resistance temperature detector. Both sensors derive from NIST-
certified (USA National Institute of Standards and Technologies) manufacturing processes: I include data sheets for all
sensors (see Data Description, below). Figure 5 demonstrates essentially perfect correlation of TMP117 and SHTC3 sensors
configured back-to-back in a protected housing (almost identical to bicycle) under roof-top photovoltaic panels; that data
demonstrated consistent reliable operations of both sensors over local air temperature ranges of -30oC to 40oC.

200 The SparkFun board hosting the MLX90614 also included an onboard temperature sensor; details and effective resolution of
that particular sensor remain vague (not discussed on Melexis MLX90614 data sheet, for example). All data files include
data from this additional temperature sensor designated as 'IR board', which showed very positive correlations with
TMP117 and SHTC3 sensors; readers can use or not use these accessory data. Figure 6 shows comparisons of data from
SHTC3 and TMP117 sensors: left plot shows a typical Fowler loop ride (on 25 June 2023) using SHTC3 and TMP117
205 sensors; middle plot shows a ride from Bozeman (on 27 June 2023) again using the bike-mounted SHTC3 and TMP117
sensors; and right plot shows identical sensors operating underneath solar panels for the time period 19 to 26 June 2023.
These data again demonstrate consistent reliable operation of SHTC3 and TMP117 sensors.

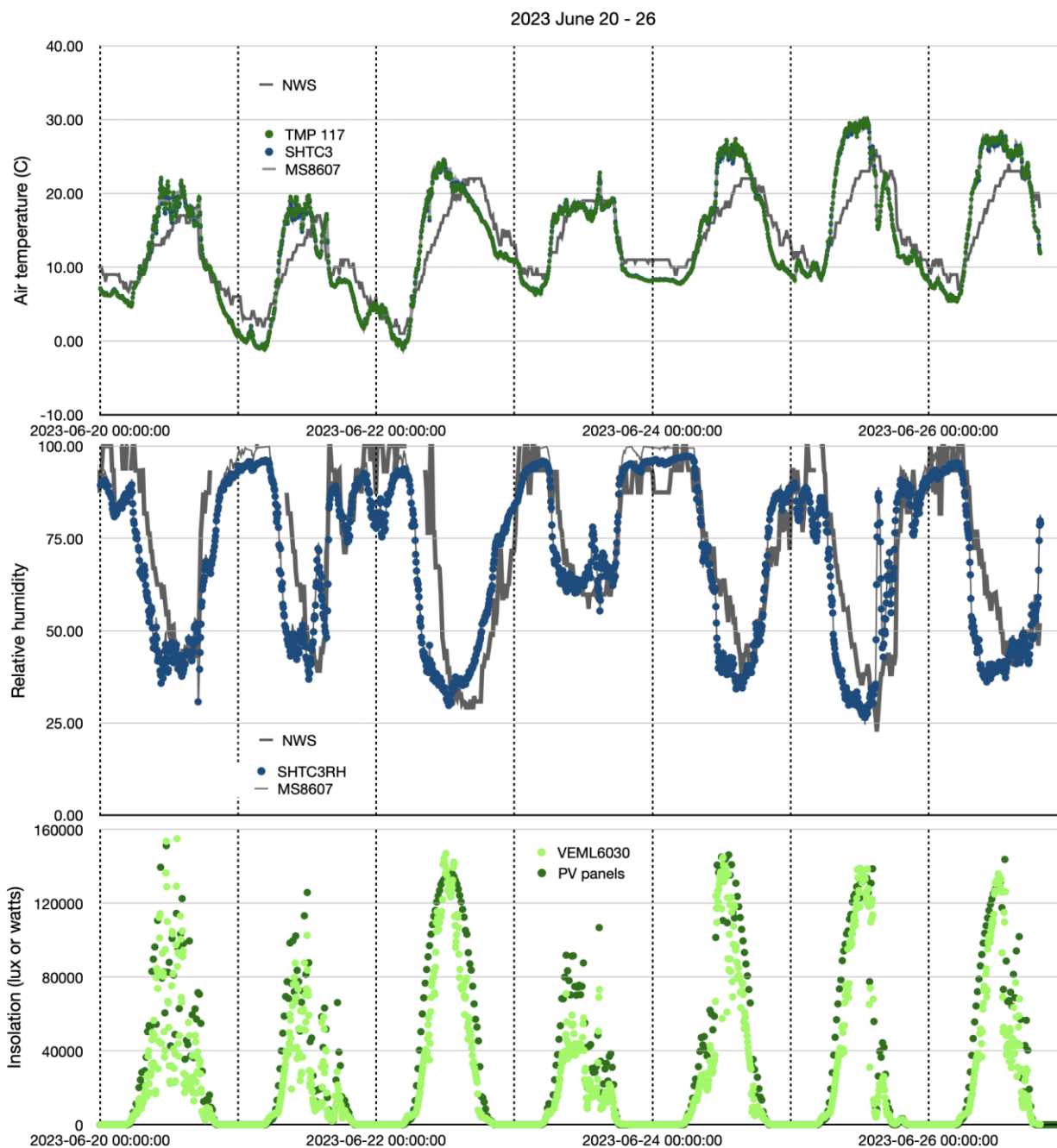
Figure 7 shows time series of air temperatures, relative humidities and insolation over the week (20-26 June 2023, also
shown in right plot from Fig. 6) for SHTC3, TMP117, MS8607, VEML6030, roof-mounted photovoltaic panels, and NWS
210 data. Temporal correlations of SHTC3, TMP117 and MS8607 data proved excellent: not distinguishable among three
sensors on these scales (top panel of Fig. 7). Correlations with distant contemporary NWS station data also proved
remarkably good, particularly when all sensors duplicated - successfully - diel patterns and amplitudes of daily temperature
or humidity increases and declines! Figure 7 also demonstrates excellent week-long correlations of roof-top insolation
(VEML6030, in lux) with roof-mounted photovoltaic panel power outputs (in watts). Readers will find details of sensor-to-
215 photovoltaic panel comparisons in Appendix E.



220 **Figure 5: Temperatures as measured by SHTC3 (vertical axis) vs. TMP117 (horizontal axis), across a temperature range of -30 to +40; that range covers all conditions encountered during these bike rides. Data files cover January 2023 through March 2024. Relationship slopes did not deviate from 0.99 while most correlation coefficients equated to 0.999 (with one lower R2 value of 0.996). Statistically, SHTC3 and TMP117 produced comparable reliable temperature data.**



225 **Figure 6: SHTC3 vs. TMP117 correlations for three different days and sources. Left: A late day Fowler loop ride, 25 June 2023, after rain. Middle: A morning southbound Bozeman-toward-home ride, 27 June 2023. Right: A week's worth of roof-top data. Note smaller 3σC ranges (18-21oC, 15-18oC) for bike rides (left, middle) compared to broad range (-5 to +30oC) for week-long (right) data. Linear correlation equations and correlation coefficients very high in all cases! Location does not change for roof-top data. Each bike-based data file includes GPS-derived locations and times.**



230

Figure 7: Time series from roof-mounted temperature, humidity and insolation sensors plotted together with temperature and humidity data from nearest NWS station (distant by ~250 meters vertical and ~24 km horizontal). Roof-mounted data include SHTC3, TMP117 and MS8607 sensors; the MS8607 sensor (data sheet available) recorded lower-resolution temperatures (+1.0oC over the range -40 to +85oC). This week-long intercomparison also included a fully-exposed VEML6030 (identical to bike-based unit) mounted parallel to photovoltaic panels, plus 15-minute power records (via SolarEdge web-based interface) directly from photovoltaic panels (details in Appendix E).

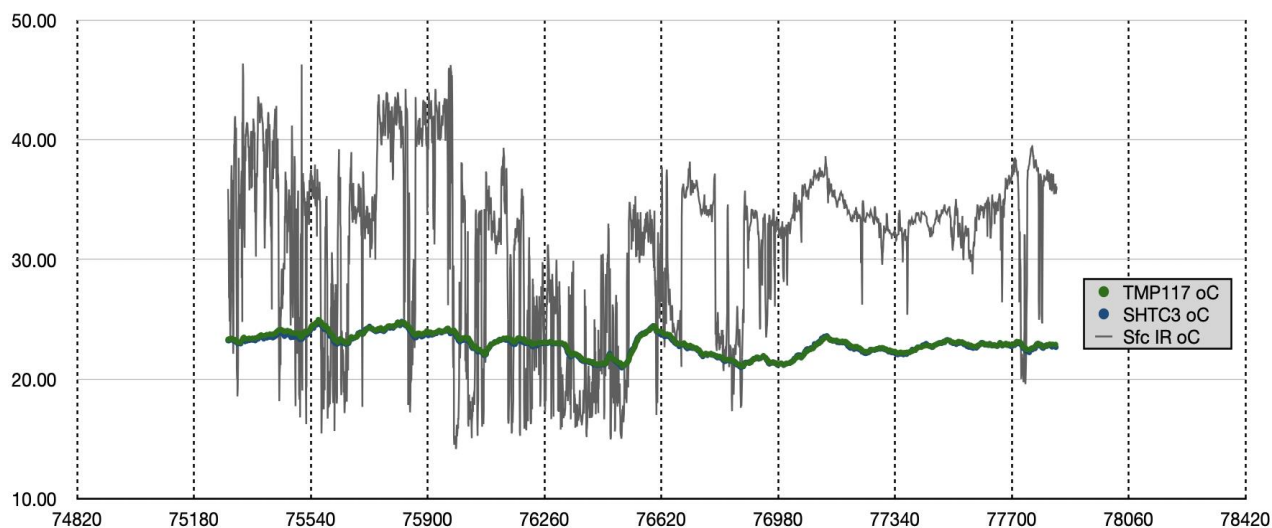


4.3 Surface (pavement) temperatures

235 I measured surface temperatures using a downlooking MLX90614 infrared (IR) thermometer on a Sparkfun board that included microprocessor, bootloader, status LEDs, communication ports, etc. The MLX90614 sensor itself, from Melexis (global), operated over the range -70 to $+380^{\circ}\text{C}$, with 0.5°C accuracy over a narrower range of 0 to $+50^{\circ}\text{C}$. MLX90614 sensors (data sheet available) allow non-contact temperature measurements in a wide variety of medical and remote sensing applications; abundant reports document applications of MLX90614 to remote sensing of human body temperatures, even to skin-based virus (Covid) detection (e.g., Constanzo & Flores 2020). With a wide field-of-view (90° for MLX90614BAA), mounted 70 cm above pavement surfaces, this IR sensor measured surface temperatures within a 1.4 meter circular footprint which necessarily included a small portion of the bicycle front wheel. A constant portion of a rapidly-rotating wheel within the sensor field of view should present no interference to measurements of surface temperatures. Starting or ending loops, which showed no statistically-valid perturbations, would have exposed wheel-induced directional or rotation-speed factors.

240

245 All subsequent analyses of this data ignore that small feature. Figure 8 shows typical output from the MLX90614 IR surface temperature sensor.



250 **Figure 8: Air and surface temperatures, 6 September 2023.** Air temperatures from TMP117 and SHTC3 sensors, indistinguishable in this figure. Surface temperatures from MLX90614 IR sensor. Data collected along same Bozeman southbound (town-toward-home) route shown in Fig. 1. Readers will quickly notice, well within 0.5°C uncertainty, MLX90614 data showing initial warmer-than-air pavement temperatures, followed by stretches (75400 to 76500 seconds) of shaded gravel paths (interspersed with travel along paved streets), succeeded eventually by long stretch along south 3rd with, again, warmer-than-air surface temperatures; short isolated patches of deep shade exist near end of the ride, inducing small patches of cooler IR surface temperatures. Gridlines along X axis mark 6-minute time stretches, each containing roughly 500 recorded data points.

255

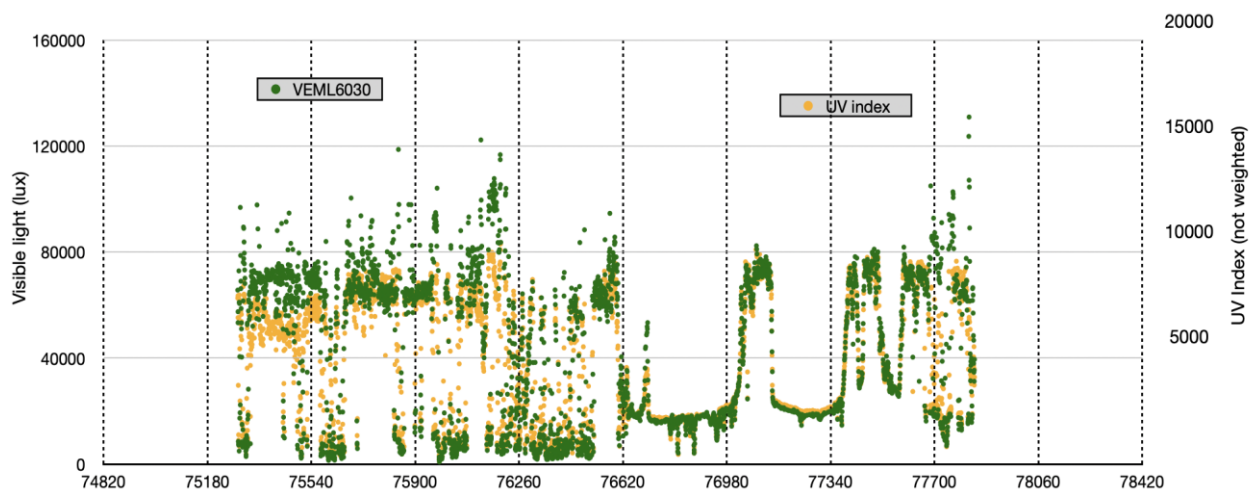


4.4 Relative humidity

Data sets include relative humidity (RH) values from the Sensirion SHTC3 sensor: +2% RH over humidity range of 0% to 100% (details in SHTC3 data sheet). Humidity data from this bicycle-mounted sensor, along with humidities reported by
260 roof-mounted SHTC3 (and MS8607), provided important temporal and amplitude verification when compared to humidities measured at a nearby NWS station. As for air temperature data, SHTC3 RH data in comparison with MS8607 data and NWS data showed excellent magnitudes and timing of diel excursions (Fig. 7).

4.5 Visible light

Data files include visible light measurements (in lux) from a 16-bit VEML6030 ambient light sensor from Vishay
265 Semiconductors (USA), manufactured for use in consumer mobile devices and displays. With a broad thermal operation range (-25oC to +85oC), the VEML6030 records light of wavelengths 450 nm to 750 nm with a response curve nearly identical to that of many human eyes. For outdoor use, often in full sun, I operated the VEML6030 with a gain of 0.125 and an integration time of 25 milliseconds; at these settings VEML6030 measurements typically maxed out at 160,000 lux. I compared bicycle-mounted VEML6030 data to data from an identical fully-exposed VEML6030 sensor, mounted beside and
270 parallel to roof-top photovoltaic panels, as well as to 15-minute records of power generated (watts) by the photovoltaic panels (Fig. 7; find intercomparison details in Appendix E). Roof-mounted VEML6030 data compare very well with photovoltaic data (Fig. 7) while VEML6030 data from the bicycle provide useful records of insolation during a ride accompanied by immediate data on tree- or rider-induced shading (Fig. 9, Appendix E).



275 **Figure 9: Bicycle-measured visible (VEML6030, in lux) and ultraviolet (UV, VEML6075, in uw/cm²) data on 6 September 2023, along same southbound route as shown in Figs. 1 and 8). Visible and UV sensors show very clear responses to time-dependent light increases (gradual increase of ‘maximum’ levels from 75000 lux to greater than 80000 lux), to intermittent full sun and full shade, to clouds (rounded transition edges), etc. Isolated patches of deep shade near end of ride show very clearly in these data. Time axis parameters identical to those in Fig. 8: UTC, GPS seconds, 6 minutes (~500 records) between vertical gridlines.**

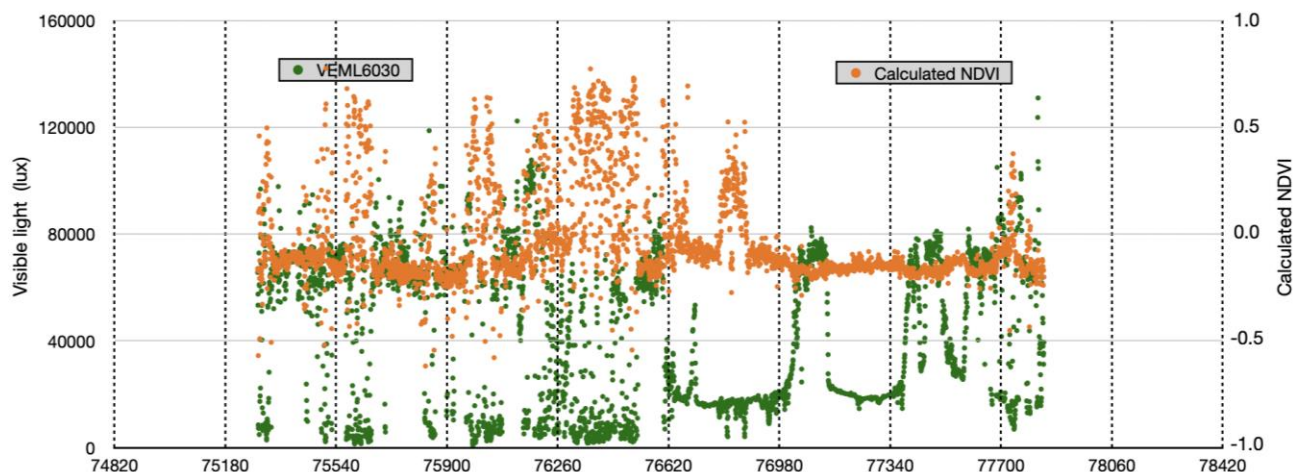


280 4.6 UV light

Data files include ultraviolet (UV) irradiance at two wavelengths (UVa 365 + 10 nm and UVb 330 + 10 nm) from Vishay Semiconductors VEML6075. This unit operates from -40 to +85°C while allowing users to combine UVA and UVB into a numeric UV Index (Fig. 9). Please note: UV index data shown here do not include wavelength-dependent weighting factors nor susceptibility factors. These basic data remain valid and useful, particularly as back-up to and confirmation for
285 VEML6030 Vis data; users may calculate UV exposures for specific locations and elevations, corrected for local cloudiness, according to appropriate national or international guidance.

4.7 Near-infrared spectral measurements

Data files include red to near-infrared (NIR) absorbance data from 610, 680 and 860 nm, all with 20 nm full-width half-max (FWHM) spectral resolution. These data come from a downlooking small stable AS7263 sensor unit from ams AG (Austria)
290 which detects sunlight reflected from underlying surfaces. Users can evaluate data at 610 and 680 nm to determine slopes of red end of visible spectra or to estimate overall spectral shapes. Using data at 680 and 860 nm, I calculated an equivalent normalized difference vegetation index (NDVI, see Appendix E for calculations) with implications for remote sensing measurements over road and other impervious surfaces; normalization during NDVI calculations plus comparisons with time of day and incoming sunlight (VEML6030) can prove useful in understanding spectral data. Figure 10 shows, again for the
295 southbound ride on 6 September 2023, NDVI calculated from 680 nm and 860 nm data (as described in Appendix E), compared with total sunlight (from VEML6030); NDVI calculations covered, on this particular ride, paved, graveled and grassy surfaces.



300 **Figure 10: Normalized difference vegetation index (NDVI) calculated from spectral data at 680 and 860 nm, along southbound bicycle ride on 6 September 2023. Lux (insolation) data from VEML 6030 exactly as in Fig. 9. NDVI from spectral wavelengths measured by AS7263. Normalization results in relatively-flat slightly negative NDVI values over impervious surfaces with strong positive excursions in shaded areas. X-axis exactly as in Figs. 8 and 9, with gridlines every 6 minutes.**



4.9 Microcomputer, software and temporal resolutions

I used a 600 MHz ARM Cortex-M7 Teensy 4.1 (<https://www.pjrc.com/teensy/>) to run all systems and to collect (on microSD
305 card) all data; this Teensy 4.1 microprocessor provided accessibility and reliability to the full system. I used standard C++
libraries (from Sparkfun in support of each sensor or from GitHub likewise) compiled within the Arduino IDE programming
environment. In many cases, after interconnection of the full suite of sensors, I could run sensor-specific example codes to
check, in sequence, operation of each sensor. In the case of the MLX90614 sensor, I used a library from Adafruit (likewise
available on GitHub) in preference to the Sparkfun library. A typical data file from a Fowler loop data ride, collected at 1.5
310 Hz, amounted to roughly 400 kB (4000+ records) across 16 variables (15 without TMP 117 before 2022-11-18): GPS
seconds, lon and lat from u-blox GPS; six records (five without TMP 117) from temperature and humidity sensors [Tsfc-Tair
calculated]; seven data records from optical sensors [including calculated NDVI]. As already mentioned, these as-recorded
data include no averaging, interpolation or other data processing.

Data sheets show that sensors had potential to operate - on their own, isolated from others - faster than several Hz. Even the
315 u-blox GPS unit advertised raw position update rates of 20 Hz or faster. In this configuration, however, after sensors
received suitable warm-up, performed - when necessary - various boot-up steps, and as the moving u-blox GPS maintained
adequate synchronization to acceptable satellites, actual recording times included individual sensor signal processing,
transfers via I2C bus, writing times via a microSD drive, etc. Those combined processing steps resulted in minimum total
data record processing times very close to 1.5 Hz. By adopting new libraries and improving prior codes, I added (after bike
320 crash on 2022-11-18) two new sensors without impact on overall processing speeds; later I achieved data recording speeds of
closer to 2 Hz (e.g., by September 2023). Applied uniformly, 1.5 Hz at 5 m/s implied spatial resolutions near 4 meters, more
than sufficient to document surface features observed here. Bicycle speeds varied, particularly descending versus ascending,
so GPS-based time and location data as trigger for each sensor-based record provided actual valid spatial resolutions. As
demonstrated above (legend to Fig. 8), below (e.g., Figs. 14, 15, 17, Appendix D), and in demonstration video
325 (<https://youtu.be/nMjBFbXxNWU>), these data at these spatial resolutions allowed easy determination of surface
temperatures along impervious or pervious roads, streets, lanes, paths, etc., with rare small residual uncertainties.

4.10 Winter-time walking data

During winter, with snow-packed or icy roads, I walked this bicycle - carrying exactly the same sensor box and using same
Garmin 830 cyclometer - along Jade Street. This short stretch of not-much-traveled rural pavement included hard-packed (by
330 vehicles or snowplows) snow and ice, particularly at the tree-shaded east end, occasional occurrences of fresh untracked
snow, and melting wet or bare pavement in sun-influenced central sections. Users should examine various still images (see
Data Description below), Appendix F and demonstration video (<https://youtu.be/nMjBFbXxNWU>). I completed westward-
then-eastward walking deployments, generally covering nearly 0.8 km with loops at both ends, within 10 minutes. In all
cases I collected data identical to bicycle rides. On one occasion (16 April 2023) I walked along Jade Street then rode around
335 Fowler loop. I also encountered snow or ice during 'regular' bicycle rides but generally in small patches easily avoided or



surmounted. On only one occasion (18 November 2022) did I fall due to slippery surfaces. During recovery from that event I added TMP117 sensor and updated acquisition codes.

5. Data uses

Data presented here cover 110 complete rides around Fowler loop (excluding interrupted partially-completed ride on 18 November 2022), 61 rides to or from Bozeman proper, plus 31 winter-time walks along snow-covered Jade Street. Readers will quickly notice three distinguishing features:

- 1) In no case did air temperatures respond to surface temperatures. When, in rare cases, I observed apparent air temperature responses to warmer surfaces, those responses never occurred consistently: too often one modest positive correlation would sit adjacent to areas of no or even negative correlation. Conversely (and rarer yet), when warm or cool patches occurred in air temperature records (these occasions often occurred after dark, see data for 2023-06-15 or 2023-08-23), the air temperature features occurred without impact on surface temperatures. Insolation (or, conversely, tree-induced shading) forced surface temperatures while - as a general case - air temperatures remained largely immune to surface influences.
- 2) Gravel (pervious) surfaces always proved cooler than paved (impervious) surfaces. At periods of maximum impervious surface temperatures (e.g., $> 25^{\circ}\text{C}$), with impervious and pervious surfaces both exposed to full insolation, graveled surfaces proved at least 5°C cooler.
- 3) Tree-induced shading, particularly dense multi-hour and multi-season shade, always resulted in cooler surface (paved as well as graveled) temperatures. Due to generally dry climate in this portion of Montana, where trees often grow along (and provide shade to) streams or irrigation ditches, one requires systematic data such as these to sort shade and waterway influences.

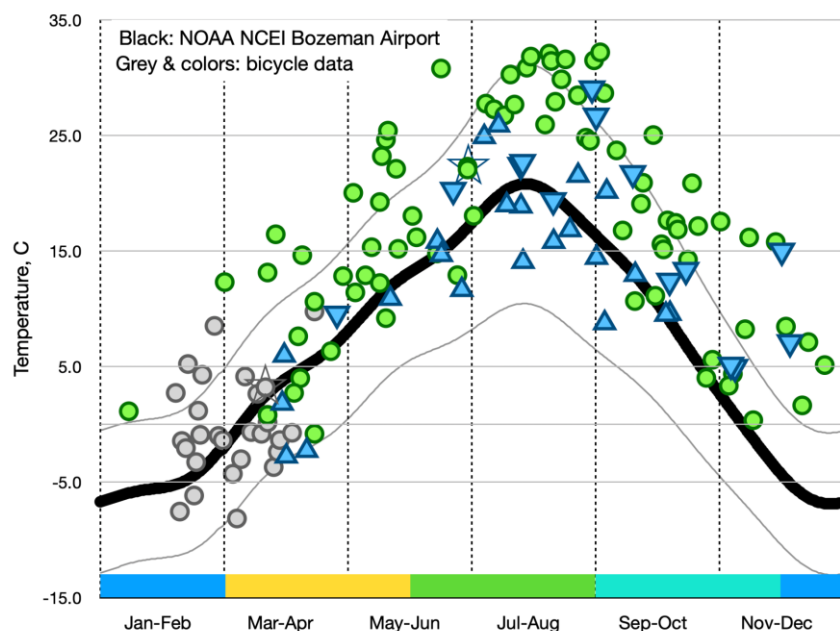
I offer examples intended to stimulate questions, explorations and replications. I address a series of validation questions.

- 5.1 How did these data compare to 'official' NWS data?
- 5.2 How did bicycle data compare to local roof-based data?
- 5.3 What maximum and minimum $T_{\text{surf}}-T_{\text{air}}$ occurred? When, where and why?
- 5.4 How did gravel surfaces differ, thermally, from paved surfaces?
- 5.5 What happened in fully (day-long) shaded areas? What happened when shading occurred for only parts of a day?
- 5.6 What happened as snow or ice accumulated, compressed and then melted?

Prospective users might raise additional questions about durability of specific sensors. I address repeatability and reliability questions in Appendix G.



365 5.1 Validation of these data against USA National Weather Service (NWS) records



370 **Figure 11:** Average (over 8-15 minutes) air temperatures from bicycle sensors compared to climate-quality data from nearby US
NWS station at Gallatin (Bozeman) Airport. NWS data from NOAA NCEI, 27-year average (1991-2018, USW00024132,
<https://www.ncei.noaa.gov/access/us-climate-normals/>) quality-controlled air (2 meter) temperatures showing daily averages
(central black line) plus daily maximum and minimum (upper and lower narrow black lines). All non-winter data come from
375 identical route along south 3rd Avenue (see Fig. 1): green dots from Fowler loop rides (clockwise, e.g., north-to-south along south
3rd, in all-but-one case) while blue triangles indicate Bozeman rides (upward-pointing triangles indicate northbound rides,
downward-pointing arrows indicate southbound rides). Triangles often occur in pairs: northbound (to town) ride followed by
southbound (return from town) ride. Gray dots indicate winter-time snow/ice walks. Stars indicate dates of maximum surface
375 temperatures (>31C warmer than air temperatures on 30 June 2022, starred green dot) and minimum (<-14C relative to measured
air temperatures on 23 March 2023, starred gray dot). Colored bars along horizontal axis denote climatological periods:
December-January-February (DJF), March-April-May (MAM), June-July-August (JJA) and September-October-November
(SON).

As mentioned above (legend to Fig. 7), the nearest long-term ‘official’ data come from a USA National Weather Service
380 (NWS) station at Bozeman airport 24 horizontal km and 250 vertical m from Jade Street. Figure 11 compares bicycle-
derived air temperature data, collected bidirectionally along south 3rd Avenue, to ‘climate-quality’ data from the NWS
station. Readers should extract two preliminary conclusions:

- This bicycle-sensor air temperature combination successfully recorded data from March to November (with a few
data-gathering rides in DJF as permitted by weather) with outcomes acceptably close to distant airport-based NWS
385 data. As intended, winter bicycle walks in February and March of 2023 added useful air temperature data collected
during ‘winter’ seasons. Considering brief collection periods of bicycle-based data, often gathered during maximum
diel illumination periods, their correspondence with distant ‘official’ multi-year NWS data, particularly with NWS
daily maximum records, proved remarkably good (Fig. 11).

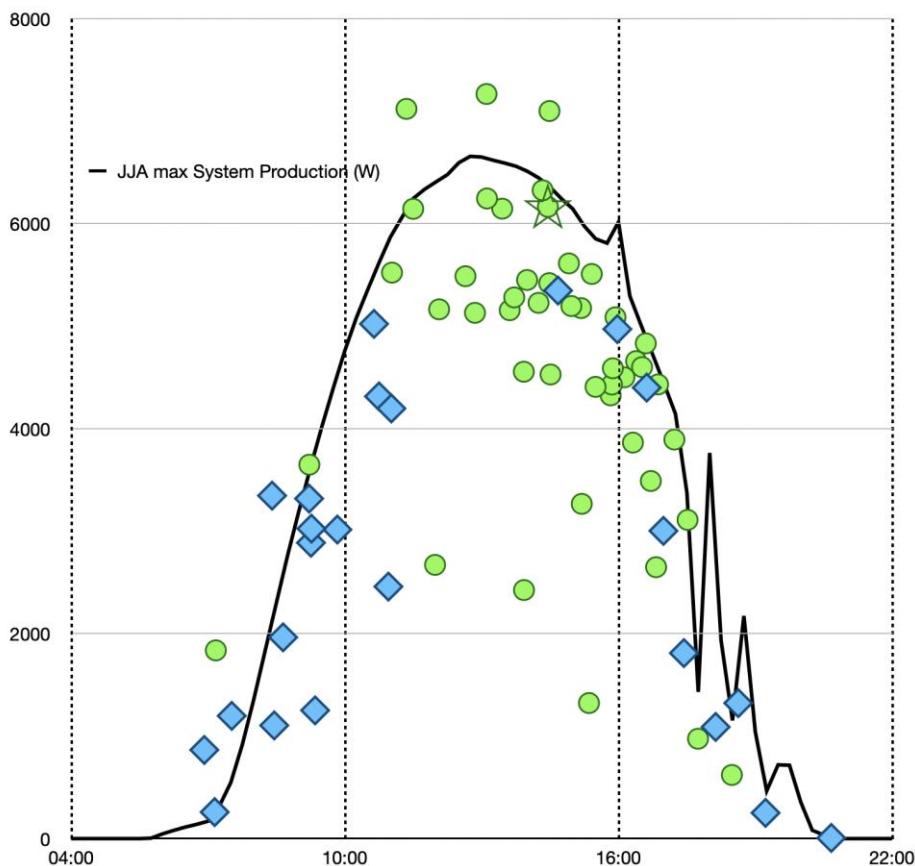


- 390
- Temperature sensors on the bicycle reproduced local ‘official’ annual data with very high fidelity. Extracting only data recorded along a frequently-riden 3-km stretch of open road, thereby avoiding deeply shaded or graveled surfaces, produced remarkable correspondence to weather service records.

Acknowledging excellent sensor-to-sensor intercomparisons (e.g., Figs. 5 and 6) plus very positive temporal correspondence of bicycle temperature sensors with local roof-mounted and distant appropriately-housed NWS sensors (e.g., Fig. 7) over weeks of data collection time, one concludes that these bicycle-carried sensors provided highly accurate temperature measurement capabilities. Minor vertical corrections (e.g., <1 m for bicycle compared to ‘official’ 2 m heights for NWS data) probably prove inappropriate in these cases, particularly in view of short durations of bicycle-based data plus interventions by other (bicycle motion, horizontal distance, elevation offset, shading, surface type) factors; any such minor ‘correction’ would only improve already-good correlations. Location-based elevation changes, e.g., drop of approximately 50 meters from SE to NW corners of Fowler loop or of greater than 120 meters to many locations in Bozeman proper, probably had greater impact than specific bicycle-based vertical sensor heights. In these locations and for these types of deployments, additional publicly-accessible validation records seem scarce at best, perhaps even non-existent. More recent climate warming impacts, as those emerge within longer-term NOAA NWS records, will also improve intercomparisons. I address longer-term repeatability and reliability of these measurements in Appendix G. In general, I conclude: use of these sensors for bicycle-based measurements of air and surface temperatures proved reliable and appropriate. Users can easily access these data to confirm or contradict.

5.2 Intercomparison of bicycle-based data ‘snapshots’ to daily and seasonal patterns of insolation, including from roof-top photovoltaic panels.

Figure 7 demonstrated excellent temporal and amplitude correlations between roof-based sensors (identical to bicycle-based sensors), NWS sensors, and roof-based photovoltaic panels, across a week of 5-minute (rooftop sensors) and 15-minute (NWS) data. In general, bicycle data came from rides during hours of 1000 to 1600 or 1700 local time; I often rode early toward town but rarely started a ride before local dawn and rarely rode after local dusk. By combining errand-driven rides (to and from Bozeman) with data-focused rides (Fowler loop), I managed to cover most daylight hours, producing excellent temporal correlations of bicycle-measured insolation maxima with nearby roof-top solar power generation records (Fig. 12). Appendix B shows similar ride distributions with consistent diel patterns for March-April-May (MAM, 36 total rides across 2022 and 2023, Fig. B1) and September-October-November (SON, 56 rides from 2021-2023, Fig. B2). During December-January-February (DJF) of 2022 and 2023 I rode only five Fowler loops plus four rides to or from Bozeman. Figs. 12 and B2 hint at behavioral patterns: Bozeman (errand) rides early with most Fowler loop (data-focused) rides occurring later. Insolations recorded by bicycle-based sensors at 1.5 Hz rarely exceeded 15-minute roof-top power generation data; bicycle-based data lower than maximal roof-top power data indicated cloudy, shaded or (rarely) rainy conditions. I gathered valid data using this bicycle over most daylight hours during most seasons.



425 **Figure 12: Maximum illumination values from bicycle-mounted VEML 6030 sensor sorted by start times for bike rides around**
Fowler loop (green dots) or to-from Bozeman (blue diamonds), compared to maximum power records from roof-mounted
photovoltaic panels, for all June-July-August (JJA, climatological northern hemisphere summer) data from 2022 and 2023.
Photovoltaic data, recorded as 15-minute power output summaries (solid black line), came from 2023-07-23; those data show
typical morning insolation followed by afternoon cloudiness. Bicycle data represent maximum illumination data, in lux, measured
during full rides, e.g. not restricted to oft-riden stretch of pavement on south 3rd Avenue. Data gathered from shaded stretches of
430 **pavement should have no impact on ride maxima. Star (on green dot) highlights the ride on which maximum $T_{sfc-Tair}$ occurred:**
 $>31^{\circ}\text{C}$ on 30 June 2022.

5.3 Average, maximal and minimal surface versus air temperatures

$T_{sfc-Tair}$ values, covering more than 600k individual GPS-located records, including data collected during winter walks along Jade Street, ranged from a low of approximately -14°C (Jade Street walk) to a high of greater than 31°C (Fowler loop ride). Parsed by date and time of bicycle ride/walk, over a total of 202 bicycle-based data-gathering rides and walks (this
435 total includes all 171 Fowler and Bozeman complete rides plus 31 winter walks along Jade Street), 45 (22%) had mean $T_{sfc-Tair}$ temperatures $> 15^{\circ}\text{C}$ (these means cover all data points collected within a ride, including partial shade, deep shade, wet spots, etc.) while 31 (15%) had mean $T_{sfc-Tair}$ temperatures below 0°C (percentages and averages calculated from Google spreadsheet table as described in Appendix A). Figure 13 demonstrates frequency distribution of mean $T_{sfc-Tair}$ values



440 during the period September 2021 to October 2023. Again, mean data cover full rides including all types of surfaces:
predominantly impervious pavement but also pervious gravel and grass-lined tracks, gathered in full sun or shade, including
snow and ice, etc. Clearly, warmer temperatures of all impervious and pervious surfaces (surface temperatures warmer than
air temperatures) dominate; an overall mean of all ride-based means equates to 7.76oC (Fig. 13). Such dominance conveys
partly-relevant information however; one must also account for percent impervious versus pervious surfaces plus effects of
day-long or intermittent shading. One can report, with confidence, that surface temperatures minus air temperatures covered
445 a relatively wide range in these data, converging around average warmth for all surfaces at all seasons of roughly 8oC.

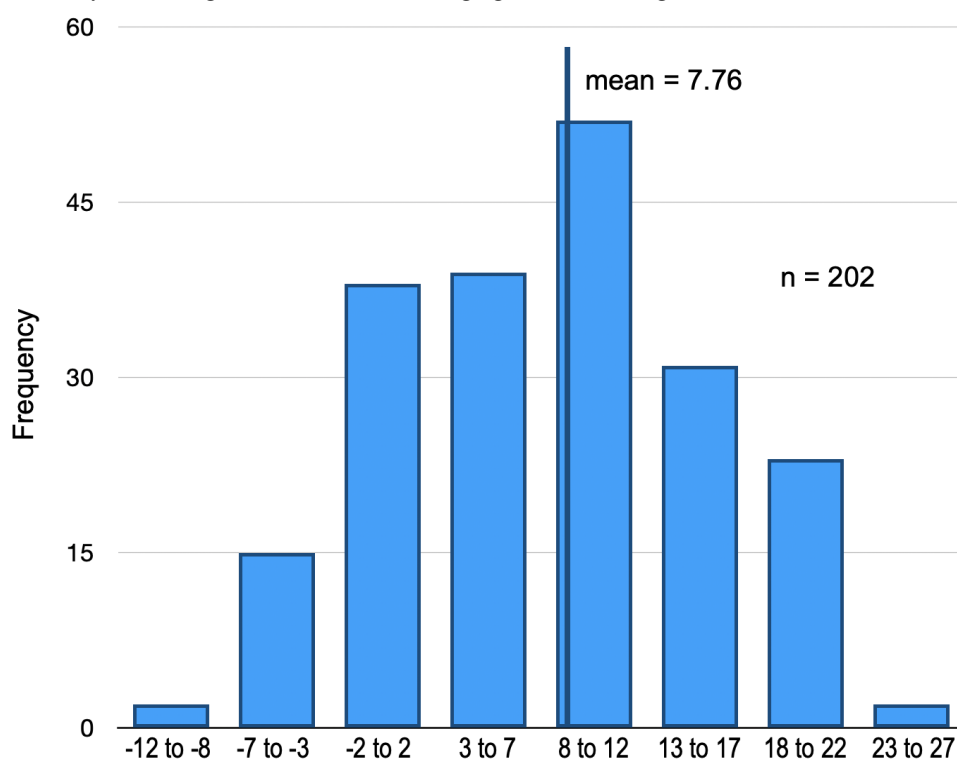


Figure 13: Frequency distribution of mean Tsfc-Tair data for 202 data records: 171 Fowler loop or Bozeman rides plus 31 winter-time walks along Jade Street. Column labels rounded to integer units (-2 to 2); actual sorted values cover 5 units (-7.5 to -2.5, -2.5 to 2.5, 2.5 to 7.5, etc.) Mean of all data = 7.76 oC (solid line).

450 Evaluation of data on maximum and minimum Tsfc-Tair temperatures proved more instructive. Maximum Tsfc-Tair
(~31.0oC) occurred on 2022-06-30 just after turning east on Patterson Road near the NW corner of Fowler loop (Fig. 14a). A
surface temperature maximum (> 30oC) occurred again in that same location (Fig. 14b) during a subsequent CCW ride along
the identical route as well as just west of (during rapid descent from) a deeply-shaded surface temperature minimum (Fig.
14c). Long unshaded stretches of both Fowler Road and south 3rd showed very warm Tsfc-Tair temperatures, whether riding
455 CW or CCW, on that particular day (users can open that day's Fowler loop data in QGIS to confirm). Ridden either direction
(e.g., all panels of Fig. 15), surface temperatures averaged almost 25oC warmer than relatively stable air temperatures of 23-
24oC on that day; actual surface temperatures greater than 50oC occurred frequently while air temperatures showed no



similar excursions (15c). Taking into account paved, graveled and shaded surfaces, JJA average maximum surface increments of 21oC over averaged air temperatures of 25oC resulted in average maximum surface temperatures of 46oC for those NH summer rides. A few reports (e.g., Pomerantz et al. 2000) record similar ‘peak’ surface temperatures for ‘warmest’ day(s), without sharing data.



Figure 14: Images of bicycle data from QGIS files. 14a: 2022-06-30, CW, NW corner of Fowler loop. 14b: 2022-06-30, CCW, NW corner of Fowler loop. 14c: 2022-06-30, CCW, near SE corner of Fowler loop. Each data point demonstrates $T_{sfc} - T_{air}$, e.g. warmth of surface versus overlying air. Data scales nearly identical in both cases: warmest colors (full yellow) indicate warmest surface temperatures: 31 to 32 C (CW) or 30.5 to 31.5 C (CCW). Nearby shade-induced lower surface temperature minimum (roughly +7 to +10 C) evident in all images. See JJA Fowler.qgis.

465 **Figure 14: Surface temperatures minus air temperatures (= net surface warming) showing individual location-based bicycle measurements for Fowler loop rides, clockwise then counter-clockwise, on 30 June 2022. Data extracted from QGIS files, against Google Earth backgrounds. Data (color) scales nearly identical in both cases: maxima of 31.5oC riding CW, maxima of 32oC riding CCW. In all cases, location of maximum surface warming ($T_{sfc} - T_{air} > 30oC$) occurred close to ‘permanently’ shaded areas of minimal surface warming. Data from QGIS analysis include toggled layers of background imagery.**

470 Users can easily calculate air or surface mean temperatures, time-of-day variations, etc. over any of several full-sun stretches (often < 1 km in length each with ~ 200 records) northbound on Fowler (as part of Fowler loop), on north- or southbound stretches of south 3rd Avenue (e.g., chosen from Fig. 1), or - in more-shaded or partly-urban settings - intermediate on north- or southbound Bozeman rides. I show here, using data from start and end loops gathered on 4 October 2022, that bicycle



direction made no difference in measured air or surface temperatures (Fig. 16); an absence of dependence of $T_{sfc} - T_{air}$ (and, consequently, of surface or air temperatures) on bicycle speed and direction persisted throughout all loops and all rides.

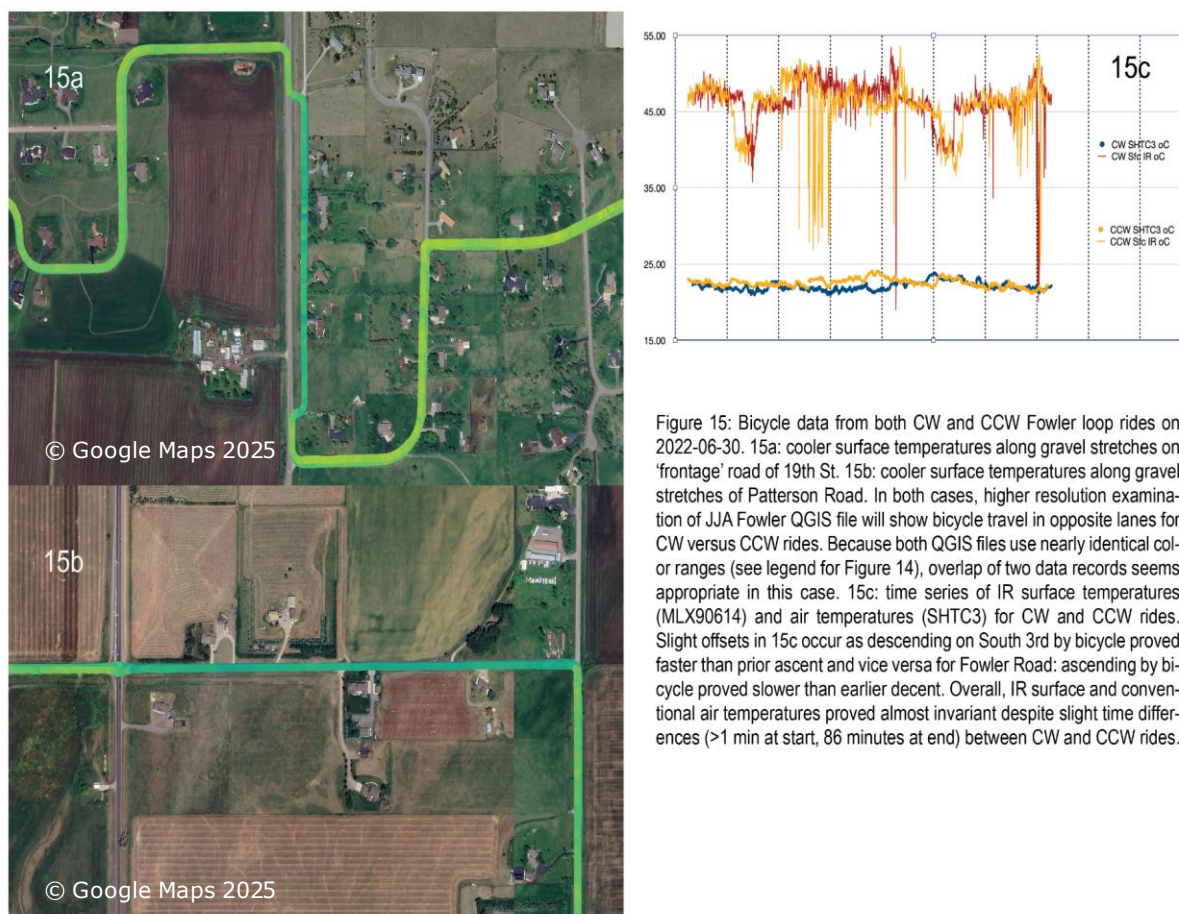


Figure 15: Bicycle data from both CW and CCW Fowler loop rides on 2022-06-30. 15a: cooler surface temperatures along gravel stretches on 'frontage' road of 19th St. 15b: cooler surface temperatures along gravel stretches of Patterson Road. In both cases, higher resolution examination of JJA Fowler QGIS file will show bicycle travel in opposite lanes for CW versus CCW rides. Because both QGIS files use nearly identical color ranges (see legend for Figure 14), overlap of two data records seems appropriate in this case. 15c: time series of IR surface temperatures (MLX90614) and air temperatures (SHTC3) for CW and CCW rides. Slight offsets in 15c occur as descending on South 3rd by bicycle proved faster than prior ascent and vice versa for Fowler Road: ascending by bicycle proved slower than earlier decent. Overall, IR surface and conventional air temperatures proved almost invariant despite slight time differences (>1 min at start, 86 minutes at end) between CW and CCW rides.

475 **Figure 15: Surface warming data ($T_{sfc} - T_{air}$) from CW and CCW rides on 30 June 2022. Because of near-identify of surface temperature maxima for CW and CCW rides, this figure includes data from both rides, overlain. Data from QGIS analysis include toggled layers of background imagery.**



480 **Figure 16: Tsfc-Tair for bicycle loops (start and end) on 4 October 2022. Values (using a single consistent color scale) showed neither directional nor start-versus-end differences. Minimal background comes from Open Street Maps selected within QGIS.**

Minimum Tsfc-Tair temperatures dropped below -14°C (relative to air temperatures of closer to 8°C) over snow-covered surfaces during a Jade Street walk on 23 March 2023 (Fig. 17). Data from this particular walk demonstrated colder surfaces at snow-covered distal ends (east and west) of Jade Street with warmer surfaces occurring in melted bare-pavement central regions (Fig. 17). The short introductory video (<https://youtu.be/nMjBFbXxNWU>) demonstrates extensive snow coverage, clear central impervious areas, plus substantial north-side to south-side differences in snow types and persistence. Taking all Jade Street walks together, data showed -3.2°C mean Tsfc-Tair for February 2023 (15 walking data measurements) but 1.9°C mean Tsfc-Tair during March (16 walks). Average Tsfc-Tair maxima for those months amounted to 5.1°C for February, 12.1°C for March. Average minima amounted to -7.5°C for February, -7.9°C for March (including -14.8°C as already noted for 23 March 2023). These data confirm a basic Jade Street pattern: cold surface temperatures at distal (especially eastern) ends, with patches of melted and occasionally dry impervious pavement covering expenses along central areas.

485
490



Figure 17: Tsfc-Tair as measured by bicycle while walking along Jade St on 23 March 2023. Data from QGIS analysis include toggled layers of background imagery.

495 5.4 Impacts of gravel

Graveled stretches proved distinctly cooler on nearly every ride (evident in Figs. 1, 8, 15, and in demonstration video), during Fowler loop circumnavigations (frontage gravel sections along south 19th St and eastern Patterson Road, e.g., Figs. 1, 15) as well as for shorter intermittent gravel sections encountered on to/from Bozeman rides (Figs. 1, 8). Data for both CW and CCW directions (Figs. 15a, b) collected on 30 June 2022 confirm this persistent pattern of cooler surface temperatures (relative to invariant air temperatures) over graveled surfaces.

As demonstrated in Figure C1 (compare to Fig. 15) spatial patterns of surface warming, shade-induced cooling, cooler gravel surfaces, etc., from a Fowler loop ride on 7 June 2023, particularly cooler pervious graveled surfaces and cooler surfaces in the presence of persistent shade, proved very repeatable. Graveled surfaces often proved $> 5^{\circ}\text{C}$ (occasionally up to 10°C) cooler than adjacent impervious pavements, without corresponding decreases in air temperatures nor - in the absence or tree shading - in insolation.

5.5 Impacts of solar insolation plus persistent versus intermittent shading

Prior work identifies light (solar insolation) as forcing function for surface heating over impervious surfaces: following pavement engineering examples (e.g., in Pomerantz et al. 2000) one might expect solar insolation to warm impervious surfaces (roads, in this case) which in turn warm overlying atmosphere. These mobile data strongly suggest a positive



510 relationship between maximum insolation and maximum $T_{sfc-Tair}$ (Fig. 18). Figure 19 confirms this insolation-forced
pattern: lowered insolation due to tree-induced shading caused spatially-confined cooling. Increased sunlight, for a few hours
at least, also induced sharper shadows (Appendix D). Results demonstrated here (discussed in Appendix D) proved
consistent and repeatable during multiple rides. These data gathered primarily over chip-sealed rural roads do not cover a
wide range of pavement albedos nor, in their immediacy, do not cover insolation occurring hours or days previously or
515 subsequently. For the most part, these data suggest relatively rapid surface heating and cooling responses, certainly within
one or two hours for heating or cooling. None of these data demonstrated persistent surface heating patterns that might lead
to heat island effects.

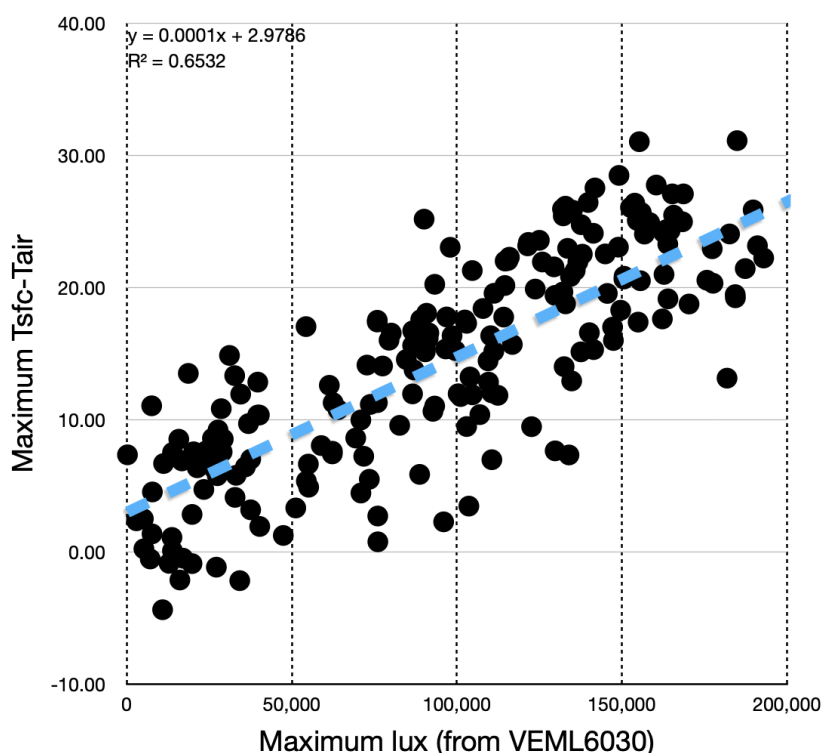
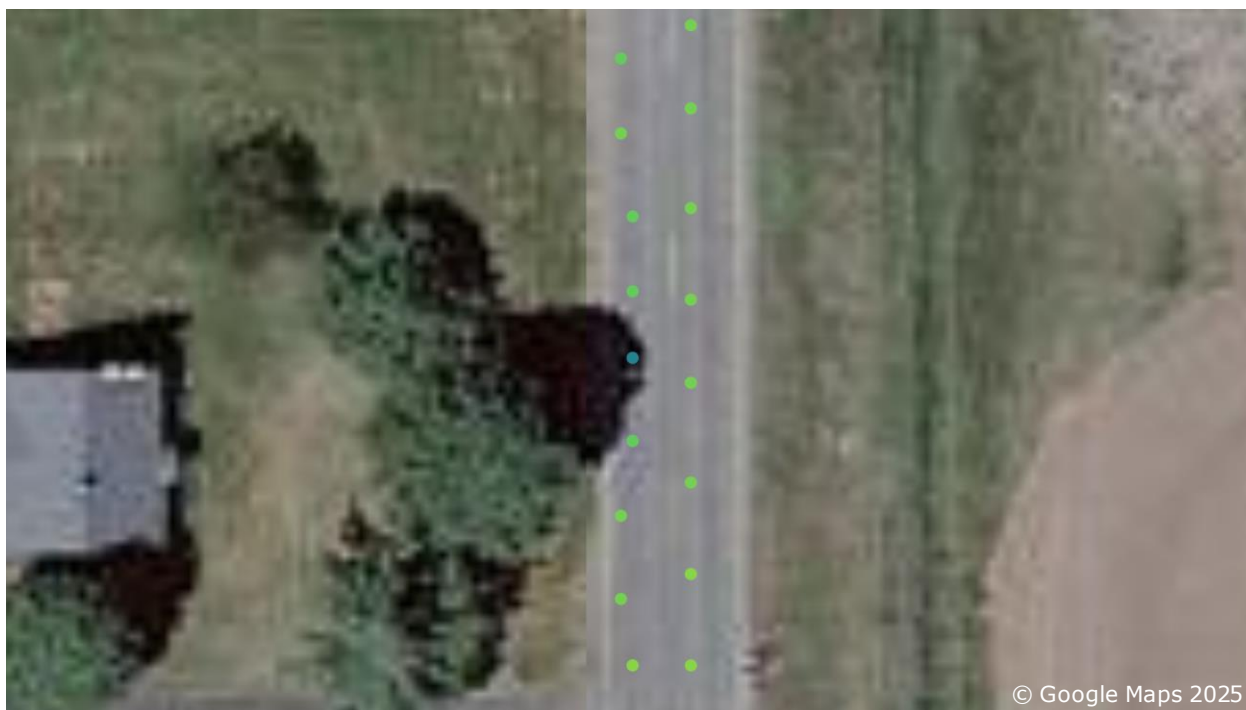


Figure 18: Maximum per-ride $T_{sfc-Tair}$ (oC) as a function of maximum insolation (lux), for all bicycle rides.

520 Insolation measurements via light sensors involve substantial uncertainties induced by spectral units, sensor orientations,
cloud cover conditions, sensor sensitivity and susceptibility, human or bicycle-induced shading, etc. Users interested in
further detail of solar insolation measured from bicycles should consult Appendix E.



525 **Figure 19: Data from CW and CCW Fowler loop rides on 30 June 2022, demonstrating shade-induced cool surface temperatures**
measured during CW loop (left track along west lane) followed (less than 20 minutes later) by identical non-shaded measurements
during CCW loop (right track along east lane). Image based on identical temperature scales northbound and southbound. Data
clearly demonstrate cooling impact extending part-way across road surface during southbound pass while northbound pass -
without shade - shows little impact. (Particular Google Earth image as GIS background recorded under very similar late-day
530 insolation conditions tends to emphasize this pattern.)

5.6 Winter conditions

As mentioned, winter conditions at this latitude, elevation and particular location often involve snow-covered, plowed, and
iced road surfaces (see for example Fig. F1). Ignoring winter-time pavement conditions thereby consigns substantial
fractions of seasonal impervious surface temperature data to obscurity. Instead, these data include same bicycle, same
535 sensors, same types of deployments, albeit by cautiously walking the bicycle back and forth along a relatively quiet section
of impervious pavement. Figure 11 demonstrates substantial impact of these walks on seasonal ranges of the overall data set.
Fig. 17 demonstrates persistent patterns of winter data: cold surface temperatures measured at snow-covered distal ends of
Jade Street with warmer surface temperatures evident in sun-exposed central sections. Users can evaluate any of 31 separate
bicycle deployments under winter conditions, covering a range of freshly snow-covered, plowed, then traveled (and,
540 subsequently, iced) surfaces. Video on bicycle and from overhead drones (recorded in <https://youtu.be/nMjBFbXxNWU>)
may prove helpful in documenting and understanding snow-covered surfaces.



6. Remaining Uncertainties

545 Details discussed above proved reliability of air and IR temperatures, RH, and light sensors deployed on bicycle for these purposes, plus distinct advantage of recording sensor data synchronously with time- and location-stamped GPS data. As hinted earlier (legends to Figs. 8, 13), users should trust individual T_{sfc} - T_{air} data points to at least $+0.5^{\circ}\text{C}$ (incorporating uncertainties of TMP117, SHTC3 and MLX90614) over average effective spatial resolution of 4 meters.

Acknowledging that bicycle speeds derived from sequential differentiation of GPS positions will vary slightly with elevation change, riding surface, tire pressure, traffic, surface wetness, rider fatigue, etc., absolute position accuracy of these data depend in part on derived GPS motions and, at least for interpretation, in equal part on imaging (satellite) uncertainties.

550 Users should check individual data carefully to understand adjacent or overlying forcing factors. Over substantial averages (distances), or in cases where neighboring features supply accurate spatial reference, users can probably regard GPS errors as insignificant; certainly < 2 m (Figs. 19 and D1a and D1c). In a few cases (e.g., Figs. 16 and D1b), users will confront > 2 meters of positional uncertainty. This author advises caution at sharp corners or as bicycle emerges from deep shade into full sun; whenever bicycle GPS data might prove uncertain (e.g., Fig. D1b) or when satellite imagery might prove mis-aligned (e.g., Fig. 16).

Do positional uncertainties as registered in Figs. 4c, 16, 17, D1 arise from GPS uncertainties or image mis-registrations or both? Where two GPS data streams agree, as happened most often - particularly on long straight sections - I assign uncertainties to mis-registrations. When one GPS position varies from another and from probable image location, I tend to adopt maximum (2 m) horizontal GPS uncertainties; users will need to make best judgements. Positional uncertainties, whether derived from GPS or imagery, had little impact on any data descriptions above. In general, particularly along 560 straight stretches in full sun, a long-track spatial resolution of roughly 4 meters will prove easily achievable and quite useful. At present, no freely-available satellite imagery, at any wavelength, coverage or repeat frequency, exceeds 10 meters of spatial resolution. As data approach meter-scale spatial resolutions, however, concerns about GPS errors versus image registration errors will prove increasingly relevant.

565 7. Implications

Surface temperature patterns observed here (e.g., sun-warmed impervious surfaces, graveled stretches cooler than pavements, shade-induced cooling) represent, individually, no surprises. These data clearly represent first 'drops in a bucket'! Other bicyclists, riding at other speeds with other sensors in other locations, might produce different outcomes, organize different intercomparisons, conduct different validations, etc. Hopefully, future riders share data!

570 These data do, however, suggest unanticipated features. First, one finds little to no indication of surface influences on overlying air temperature or vice versa. Heat island effects, much invoked (even if specific data for impervious surfaces remain mostly missing or hidden), require - evidently - longer heat accumulation or relaxation times, deeper pavement layers with - consequently - greater heat absorption capabilities, larger expanses of impervious surfaces, abundant reflective buildings, absorbent rooftops, restricted air circulations in distinctly urban settings, etc.; who knows what additional factors



575 convert patterns of quickly warming and cooling impervious surfaces such as observed here to incidences of persistently -
warm urban microclimates. As researchers explore these issues (necessarily involving satellite remote sensing) they might
need data such as these as relevant baselines.

Second, graveled (pervious) surfaces proved persistently cooler than adjacent paved (impervious) surfaces. Although gravel
surfaces present difficult maintenance challenges, particularly in urban settings, researchers need to acknowledge cooling
580 impacts. Researchers also need to address changed run-off properties for pervious graveled surfaces. Some literature exists
related to pedestrian-useful paths in urban settings; sharing one's data might prove useful to assess potential utility and trade-
offs for specific planning of such routes. Distinctly cooler gravel surfaces such as observed here might prove useful for
general urban planning.

Third, tree-induced shade can impose large impacts on diel and seasonal surface temperatures. Urban planners already know
585 trade-offs related to deciduous and coniferous trees. To evaluate cost-benefit estimations of tree-induced shading, one will
need data such as these.

Much knowledge, and such data as exist, remains unfortunately within protected urban and highway planning communities.
When useful data becomes available (e.g., to address highway freezing concerns around 0oC), it often emerges in highway
safety rather than climate contexts (e.g., Karsisto & Loven 2019). These disparate communities - of highway engineers and
590 climate researchers - might achieve mutual benefit by: a) increased data sharing; and b) attention to rural regions as
important baselines.

I stay mostly away from evaluations of calculated variables such as UV exposure or NDVI; I provide potentially -useful data
but leave contention to experts. If normalized for incoming total light, do UV data as presented here have predictive
relationship to human UV exposure? Does NDVI have any validity on these scales or in rural environments? These data,
595 voluminous for local rural roads at all seasons, might prove useful in larger remote sensing or exposure evaluations?

Could a combination such as demonstrated here - of bicycles carrying small inexpensive commercially-tested sensors - prove
useful in closing social, philosophical or environmental gaps? With cost of GPS units falling as resolutions increase, as
phones and vehicles drive sensor improvements up and costs down, and as citizens look for ways to contribute to and
explore local climate issues, bicycles might represent easy-accessible friendly options! By careful selection of sensors and
600 boxes, users could replicate these measurements for less than \$250; basic measurements require only GPS, temperature and
humidities from SHTC3, surface temperatures from MX90614, plus incoming light via e.g., VEML6030, deployed on
standard bicycles. Other researchers have used bicycles carrying (awkwardly, one must admit) 'meteorologically -acceptable'
instruments to explore urban issues (useful summary in Rajkovich & Larsen 2018). Those expensive time-limited
explorations might benefit from open assessments of innovative reliable sensors, from comparisons with rural baselines,
605 from sharing of data, and from engagement with active contingents of bicycle-based citizens. One can imagine suitably-
equipped bicycles providing spatial and temporal coverage in urban environments! Other communities (e.g., of atmospheric
chemists, c.f. Malings et al. 2024) identify advantages of multiple inexpensive sensors. Why not a similar exploration by
urban residents? Data shared here, accompanied by validations, explanations, and explicit documentation of limitations,
provides hopeful examples for next steps by an urban climate community?



610 **8. Data Availability**

All data, sensor data images, and accessory information (e.g., sensor data sheets) reside on Zenodo. These particular data, based on accurate GPS locations, cry out for geographic analyses. Users can add any data from any ride as a ‘text-delimited’ layer in any competent GIS software, then add various backgrounds (analyses shown here used Google Earth or Open Street Map), choose parameters, adjust scales and symbols, etc. I recommend free open-access highly-capable QGIS software.

615 The table below lists all sources of data, images and miscellany.

Time period	DOI	Image file DOI	Reference
Summer 2022-2023 (71 rides)	https://doi.org/10.5281/zenodo.15053252	https://doi.org/10.5281/zenodo.15053336	Carlson 2025b
Fall 2021-2023 (54 rides)	https://doi.org/10.5281/zenodo.15053261	https://doi.org/10.5281/zenodo.15053390	Carlson 2025c
Miscellaneous (53 files)	Sensor sheets, source files, pictures, etc.	https://doi.org/10.5281/zenodo.15054004	Carlson 2025d

Each .csv data file carries date and ride location information in its title (‘bike-20250228fowler’) with designations “fowler” and “bozeman” showing routes plus “north” or “south” indicating direction of Bozeman routes (south-bound if not otherwise indicated). Each .csv file (of ~400 kb holding approximately 4000 records) carries detailed header information: GPS sec
 620 (UTC), lon[gitude] (degree.decimaldegree), lat[itude] (degree.decimaldegree), TMP117 (oC) [in files after 2022-11-18], SHTC3 (oC), SHTC3 RH (%), Sfc IR (oC), IR board (oC), Tsfc-Tair (oC) [calculated], VEML6030 (lux), VEML6075 UVa (uW/m2), VEML6075 UVb (uW/m2), AS7263 A610 [absorbance], AS7263 A680 [absorbance], AS7263 A860 [absorbance], NDVI [calculated, see Appendix E]. Users can easily open .csv files in spreadsheets or GIS software or both. Please note: other than in Appendix G, all analyses reported in this paper cover only September 2021 to October 2023 data,
 625 excluding recent (2025) data.

A second set of Zenodo files, listed in table above, holds sensor screenshots to demonstrate full data records for each ride: GPS heading (top panel); SHTC3, TMP (after 18 November 2022) and MLX90614 temperatures (second panel); Tsfc-Tair (calculated using SHTC3 air temperatures before 18 November 2022 and TMP temperatures after, third panel); then visible light (VEML6030) and NDVI (calculated from AS7263 wavelengths) overlain in fourth (bottom) panel. Horizontal axes
 630 nearly always cover one hour, demarcated at 6-minute (~500 data points) intervals. Vertical axes as labeled (heading directions, temperatures, temperature differences, light levels) include approximately consistent temperature ranges (e.g., around 25 to 30 C) adjusted upward or downward - primarily according to season - as necessary for convenient display. Although generally not shown, NDVI ranges always cover 1.0 to -1.0. These images represent all-ride composites of data displayed in Figs. 8, 9 or 10. Users can easily peruse .png images to: a) visually sort within or among Fowler loops vs
 635 Bozeman routes; b) easily identify graveled stretches; c) begin to recognize time of day or intensity of sunlight by direction, length and sharpness of shadows; then d) choose a data file or files for subsequent spreadsheet analysis or GIS comparisons.



I also uploaded accessory data into a Zenodo folder entitled “Files to support bicycle data”. This folder holds bicycle and shading images, sensor data sheets and external data from local PV panels and from nearby NWS station. Users will find additional details in Appendix A. At <https://doi.org/10.5281/zenodo.15054004> (Carlson 2025d). Users will find:

- 640 • Four tree-shading images, all .png and all as QGIS image exports using Google Earth backgrounds; these time-labeled images occur in Fig. 19 and Appendix D.
- Seven .jpgs, of bike, bike boxes and snow- or ice-covered road surfaces. Users will have seen all or portions of these images in Figs. 2 and 3 above or used in Appendix F, below.
- 645 • One file - “Bike data from Google sheet” - representing a full data export, in .csv format, from the Google sheet that I use to track all rides and data files. This file contains standard columns for date, time, location, air temperatures, maximum surface temperatures, maximum light levels plus columns containing brief ride notes (‘windy’, ‘body shading’, ‘rain’). Users might, for example, choose to compare notes on direction-dependent periods of body shading with actual light data. This particular .csv file contains valid entries for all 202 bicycle rides; read details in Appendix A.
- 650 • One file - “NOAA NWS-Gallatin” - with USA NWS ‘official’ climate data (as displayed and explained in Fig. 11). I include these data in the event users encounter difficulty accessing NOAA’s NCEI data repository.
- Three files recording daily power data from local solar panels (referred to in Fig. 12 above and in Appendix B, all with relevant dates) plus one short (four-hour) record of photovoltaic power covering CW then CCW bicycle rides along Fowler loop on 30 June 2022.
- 655 • Nine files, all as .pdf, representing data sheets for all sensors described here:
 - U-blox ZED9FP GPS unit;
 - SHTC3 temperature and humidity sensor;
 - TMP 117 temperature sensor;
 - MLX90614 IR remote temperature sensor;
 - 660 ○ VEML6030 visible light sensor;
 - VEML6075 UV light sensor;
 - MS8607 pressure, temperature and humidity sensor (deployed only on local roof);
 - AS7263 wavelength-resolved near-IR sensor; and
 - FS3000 air velocity sensor.

665 As described above, I do not provide bicycle-mounted Garmin 830 files for reasons of: a) lower temporal and spatial resolution than u-blox GPS data; and b) nearly-perfect redundancy of Garmin 830 data with u-blox GPS data (e.g., Fig. 4a). I keep the entire GPS 830 set, identified for times and routes, easily available to users on request.

I have also not included FS3000 air flow sensor data. That sensor ensured airflow across shielded temperature sensors. However, extrapolation of bicycle-based airflow data to, for example, road-level wind involves documenting exact
670 instantaneous bicycle speed and direction, recording mean synoptic-scale wind fields plus known variations in space, time, and elevation, noting wind-sheltering effects of road-side trees, etc. Interested users can request FS3000 data.



9. Conclusions

Data described and available here come from a standard bicycle carrying a small low-cost highly-reliable sensor package, deployed on roads and paths of semi-rural settings during all seasons in southwest Montana. Sharing this data demonstrates range and capabilities of a bicycle, proves utility and reliability of easily-available sensors, and offers, for evaluation and use, some of the first open-access data comparing heating of impervious to pervious surfaces exposed to full sun or to tree-induced shade across snow-free and snow-covered seasons. At this moment, resolutions achieved by bicycle (4 to 5 meters) exceed resolutions of freely-available satellite data (e.g., Landsat at 30 m, Sentinel-2 at 10 m); one anticipates positive convergence in the future with bicycle-based measurements supplying ‘ground-truth’.

675

680 These openly-shared bicycle-based data should prove useful for pavement engineers as well as climate researchers. The data cover important textural and insolation differences across roads and paths near Bozeman Montana. These data do not support evaluations of urban heat island effects; they provide necessary baselines while allowing researchers to identify missing factors. I hope bicycling citizens emulate and extend these measurements.

10: Video resources

685 All readers should watch a short YouTube video at <https://youtu.be/nMjBFbXxNWU>. This video introduces bicycle and sensors, and demonstrates clear impacts of gravel, meltwater, shade, and snow and ice on surface measurements. The author holds nearly 20 freely-available video records: bike-mounted warm (summer) and cold (winter) conditions on Fowler loop and late-season wet and dry conditions on roads and paths of north- and south-bound rides to and from Bozeman. Twice (9th of February and 9th of March 2023), we combined bike-mounted video with overhead drone-captured video, always on Jade walk sections. I used extracts of these videos to prepare a ‘demo’ video uploaded to YouTube referenced above. Several video records demonstrate persistent snow-cover of local roads, including slippery conditions on 18 November 2022 that caused abrupt bicycle crash. Because of battery limitations, south-bound videos from Bozeman rarely continue onto impervious pavement along (for example) south 3rd; they do however record highly intermittent shade and pervious/impervious surfaces along ‘Galligator’ and ‘Sourdough’ (local names) trail systems. Viewing real-time video recorded during a bicycle ride can prove mind-numbing! Users with extraordinary endurance can request videos to confirm data collection conditions, explore pavement compositions, or enjoy relative absence of motorized vehicles.

690

695

11. Author contributions:

D Carlson built and tested sensors, rode his bike on all routes at all times, conducted analyses, and wrote this description.



12. Declaration about conflicts of interest

700 D Carlson declares no conflicts of interest. Prior to retirement, he, with H Pfeiffenberger, founded this journal and - for more than a decade - served as chief editor. He presently meets prior commitment by serving (as-promised) as editor for a much-delayed special issue focused on aerosols over northern Finland. He expects thorough unbiased review of this product!

13. Acknowledgements

705 Whose career, other than Dave's, includes atmospheric technology and climate? Son Sam Carlson found and assembled bike. Son Gus Carlson operated drone and recorded drone-based videos. Dave issues particular thanks to Mary Lou Carlson for decades of patience and tolerance.

References

- Brandsma, T. and Wolters, D.: Measurement and Statistical Modeling of the Urban Heat Island of the City of Utrecht (the Netherlands), *J Appl. Met. Climat.* pp. 1046-1060, <https://doi.org/10.1175/JAMC-D-11-0206.1>, 2012.
- 710 Carlson, D., Winter/Spring bicycle data and associated image files, <https://doi.org/10.5281/zenodo.15053199> and <https://doi.org/10.5281/zenodo.15053288> [data sets], 2025a.
- Carlson, D., Summer bicycle data and associated image files, <https://doi.org/10.5281/zenodo.15053252> and <https://doi.org/10.5281/zenodo.15053336> [data sets], 2025b.
- Carlson, D., Fall bicycle data and associated image files, <https://doi.org/10.5281/zenodo.15053261> and
715 <https://doi.org/10.5281/zenodo.15053390> [data sets], 2025c.
- Carlson, D., Miscellaneous files to support bicycle data, <https://doi.org/10.5281/zenodo.15054004> [miscellaneous sheets], 2025d.
- Costanzo, S. and Flores, A.: A Non-Contact Integrated Body-Ambient Temperature Sensors Platform to Contrast COVID-19, *Electronics* 9(10), 1658; <https://doi.org/10.3390/electronics9101658>, 2020.
- 720 Demuzere, M., Kittner, J., Martilli, A., Mills, G., Moede, C., Stewart, I. D., van Vliet, J., and Bechtel, B.: A global map of local climate zones to support earth system modelling and urban-scale environmental science, *Earth Syst. Sci. Data*, 14, 3835–3873, <https://doi.org/10.5194/essd-14-3835-2022>, 2022.
- Emery, J., Pohl, B., Cretat, J., Richard, Y., Pergaud, J., Rega, M., Zito, S., Dudek, J., Vairet, T., Joly, D., Threvenin, T.: How local climate zones influence urban air temperature: Measurements by bicycle in Dijon, France, *Urban Climate* 40,
725 <https://doi.org/10.1016/j.uclim.2021.101017>, 2021.
- He, W., Li, X., Zhou, Y., Shi, Z., Yu, G., Hu, T., Wang, Y., Huang, J., Bai, T., Sun, Z., Liu, X., and Gong, P.: Global urban fractional changes at a 1 km resolution throughout 2100 under eight scenarios of Shared Socioeconomic Pathways (SSPs) and Representative Concentration Pathways (RCPs), *Earth Syst. Sci. Data*, 15, 3623–3639, <https://doi.org/10.5194/essd-15-3623-2023>, 2023.



- 730 Ibrahim, S.H., Ibrahim, N.I.A., Wahid, J., Goh, N.A., Koesmeri, D.R.A., Nawi, M.N.M.: The Impact of Road Pavement on Urban Heat Island (UHI) Phenomenon. *International Journal of Technology*, 9(8), 1597-1608, <https://doi.org/10.14716/ijtech.v9i8.2755>, 2018.
- Karsisto, V. and Loven, L.: Verification of Road Surface Temperature Forecasts Assimilating Data from Mobile Sensors, *Weather Forecasting*, 34(3), <https://doi.org/10.1175/WAF-D-18-0167.1>, 2019
- 735 Lehnert, M., Kubecek, J., Geletic, J., Jurek, M., and Jindrich, F.: Identifying hot and cool spots in the city centre based on bicycle measurements: the case of Olomouc, Czech Republic, *Geographic Pannonica* 22(4), <https://doi.org/10.5937/gp22-19750>, 2018.
- Malings, C. and co-authors: Integrating Low-Cost Sensor Systems and Networks to Enhance Air Quality Applications. GAW Report 293, WMO Publications Board, 182 pp., 2024.
- 740 NOAA NCEI 27 years (1991-2018), station USW00024132 Bozeman Gallatin Field (airport). <https://www.ncei.noaa.gov/access/us-climate-normals/> (last access 21 May 2025)
- Pomerantz, et al.: The Effect of Pavements' Temperatures on Air Temperatures in Large Cities, US EPA and DoE report, 2000.
- Rajkovich, N. and Larsen, L.: A Bicycle-Based Field Measurement System for the Study of Thermal Exposure in Cuyahoga
- 745 County, Ohio, USA, *IJERPH*, 13, 159, <https://doi.org/10.3390/ijerph13020159>, 2016.
- Samad, A. and Vogt, U.: Investigation of urban air quality by performing mobile measurements using a bicycle (MOBAIR), *Urban Climate*, 33, 100650, <https://doi.org/10.1016/j.uclim.2020.100650>, 2020.
- Zhang, X., Liu, L., Zhao, T., Gao, Y., Chen, X., and Mi, J.: GISD30: global 30 m impervious-surface dynamic dataset from 1985 to 2020 using time-series Landsat imagery on the Google Earth Engine platform, *Earth Syst. Sci. Data*, 14, 1831–1856,
- 750 <https://doi.org/10.5194/essd-14-1831-2022>, 2022.
- Zhang, X., Liu, L., Wu, C., Chen, X., Gao, Y., Xie, S., and Zhang, B.: Development of a global 30 m impervious surface map using multisource and multitemporal remote sensing datasets with the Google Earth Engine platform, *Earth Syst. Sci. Data*, 12, 1625–1648, <https://doi.org/10.5194/essd-12-1625-2020>, 2020.

Appendices

755 **Appendix A: ‘Complete’ table of ride notes and summaries.**

This file, carrying the title “Bike data from Google sheet” in the Zenodo folder “Files to support bicycle data” (<https://doi.org/10.5281/zenodo.15054004>), provides a recent (March 2025) export (as .csv) from master data sheet maintained on Google drive covering summary data and notes for all rides. Header for this file includes: Date, Start time (UTC seconds), Start time (local hour/minute), Route Distance (km), Ride notes (‘windy’, ‘dusty’, ‘shaded’, ‘wet’, etc.),

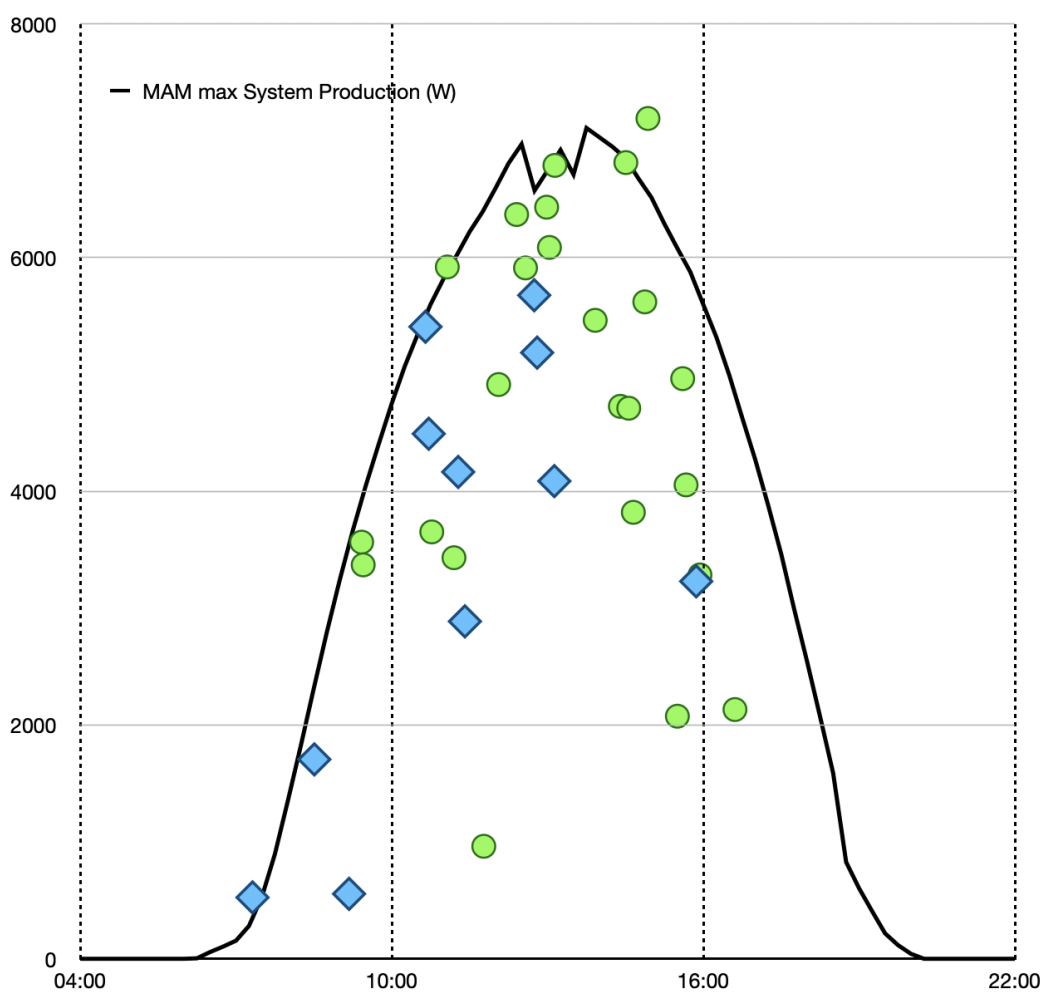
760 East/West air temp (C), South 3rd air temp (C), Sfc-air mean (C), Sfc-air min (C), Sfc-air max (C), lux (min), lux (max). In personal version (not shared) I might also track processing steps, correlation values, color code rows by season, etc. ‘East/West’ air temperatures refer to data measured during west-bound travel along Bristol Lane at the start of Fowler loops;



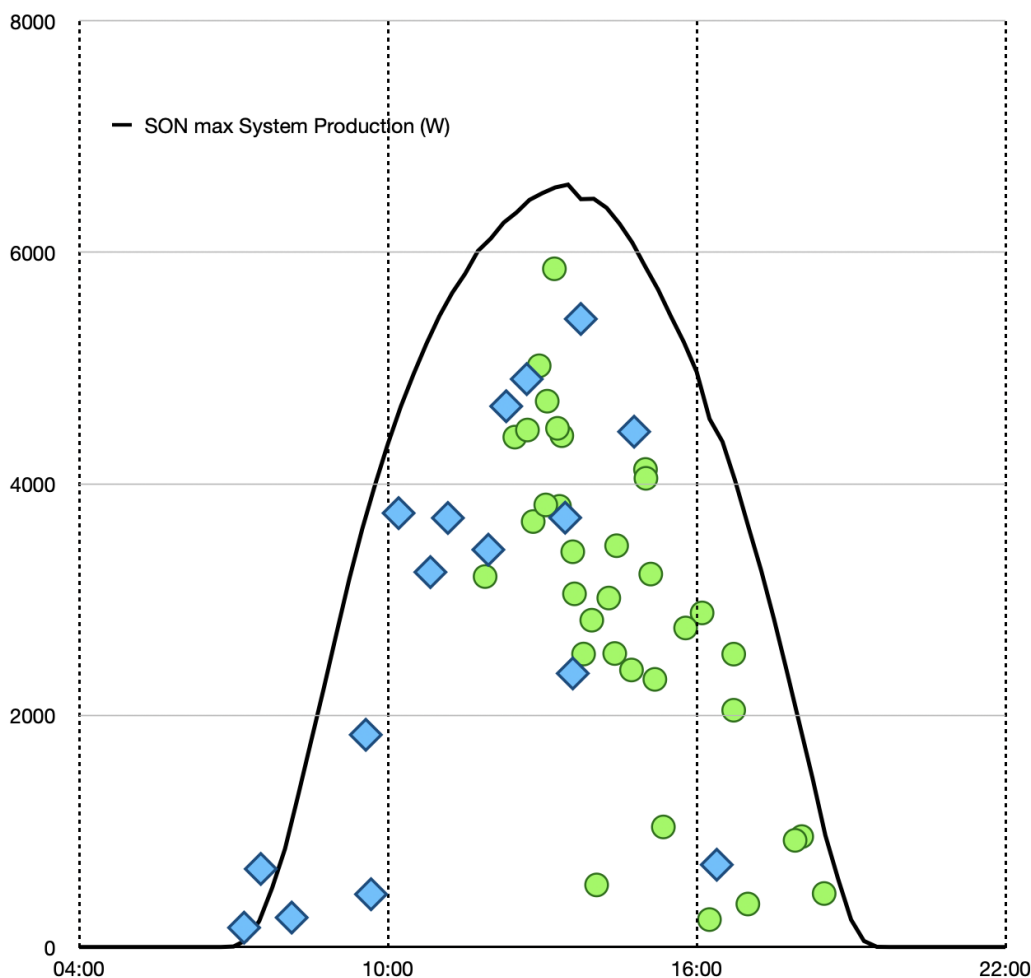
these data might hold useful insights not explored here. I share this minimal version so that users can reproduce e.g., Figs. 11 or 18. Users might also want to know local times, maximum light (lux) values, etc.

765 Appendix B: Visible and UV light comparisons and ‘validations’

These particular data (Figs. B1 and B2) supplement data presented in Fig. 12, albeit for other seasons. Due to fewer data, I have not produced a plot for December-January-February.



770 Figure B1: Exactly as in Fig. 12, but for March-April-May (MAM): maximum illumination values from bicycle-mounted VEML 6030-sensor sorted by start times for bike rides around Fowler loop (green dots) or to-from Bozeman (blue diamonds), compared to maximum power records from roof-mounted photovoltaic panels, for all MAM ride data from 2022 and 2023. Photovoltaic data, recorded as 15-minute power output summaries (solid black line), came from 2023-05-01. Bicycle data represent maximum illumination data, in lux, measured during full MAM rides, e.g, not restricted to off-riden stretch of pavement on south 3rd Avenue. Data gathered from shaded or graveled stretches of pavement should have no impact on ride insolation maxima.



775

Figure B2: Exactly as in Figs. 12 and B1, but for September-October-November (SON): maximum illumination values from bicycle-mounted VEML 6030-sensor sorted by start times for bike rides around Fowler loop (green dots) or to-from Bozeman (blue diamonds), compared to maximum power records from roof-mounted photovoltaic panels, for all SON ride data from 2021 to 2023. Photovoltaic data, recorded as 15-minute power output summaries (solid black line), came from 2023-09-10. Bicycle data represent maximum illumination data, in lux, measured during full SON rides, e.g. not restricted to oft-riden stretch of pavement on south 3rd Avenue. Data gathered from shaded or graveled stretches of pavement should have no impact on ride insolation maxima.

780

785 Appendix C: Graveled surfaces

Figure C1 demonstrates, using Fowler data from 7 June 2023 (users can monitor this discussion by looking at sensor data image from 2023-06-07), persistently cooler properties of graveled surfaces. One assumes that persistently cooler surface



temperatures for pervious (graveled) road or path surfaces versus impervious (paved) road surfaces relate to absence of asphalt binders (see Introduction and Section 5.4). In many cases, particularly along south-to-north stretches of pervious
790 (graveled) road surfaces of Fowler loop and along substantial stretches of to-from Bozeman trail rides, gravelled surfaces coincided with tree-induced shading; instances of tree shading coupled with color-than-impervious gravelled surfaces occur frequently in this data. As Figure C1 demonstrates, gravelled surfaces often showed temperatures at least 5oC cooler than adjacent impervious surfaces, and contained distinctly cooler (inverted) peaks due to tree-induced shade. In this particular situation some gravelled areas proved > 7oC cooler than adjacent impervious surfaces; other rides on other days produced
795 gravel temperatures cooler than adjacent impervious surfaces by 10oC. Cooler surface temperatures of gravelled surfaces proved pervasive throughout these bicycle-gathered data, almost always without corresponding responses (diminutions) of overlying air temperatures.

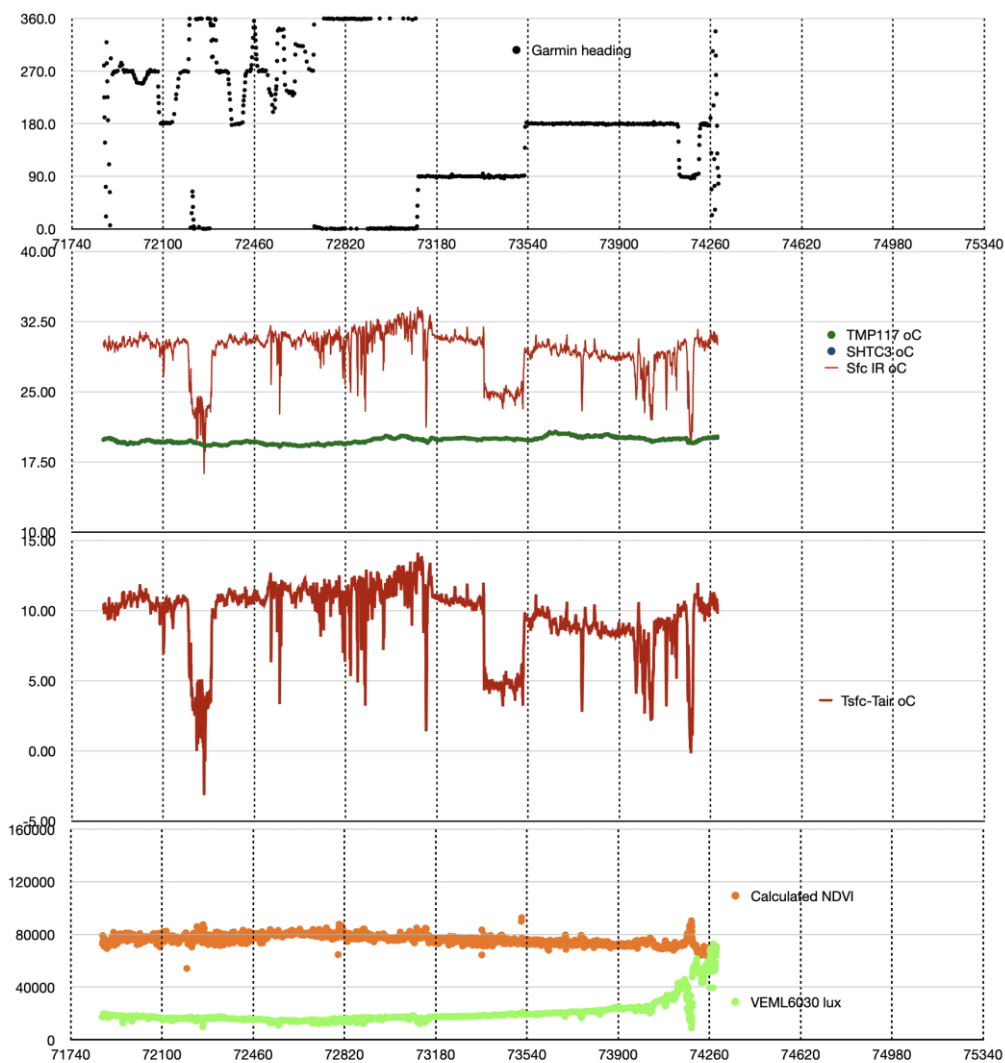


Figure C1: Data from Fowler loop ride on 7 June 2023, demonstrating cool surface temperatures on south-to-north (around 800 72200) and west-to-east (starting from ~73350) graveled (pervious) surfaces compared to adjacent impervious (paved) surfaces. As generally occurred across full data set, on this particular very-cloudy ride sensors recorded cooler gravel stretches independent of changes in air temperatures or insolation. Top panel: GPS headings. Second panel: surface (red lines) and air temperatures (blue dots from TMP117 and green dots from SHTC3, indistinguishable at these scales) plotted together over temperature range of +10 C to +40 C. Third panel: Tsfc-Tair (red lines) plotted over temperature difference range of -5 C to +15 C. Bottom panel: light data 805 (green dots from VEML6030) plus calculated NDVI (orange dots, using wavelengths of 680 and 860 nm from AS7263). Time (along horizontal axis) runs from 71740 GPS seconds to 75340 GPS seconds, 3600 total seconds, 360 seconds (6 minutes) per grid line. Fowler loop ride consumed 42 minutes to cover 15.06 km, starting from 13:56 local time.



Appendix D: Shading impacts

810 In small regions, for examples ~100 m stretches at NW corner and SW ditch/creek crossing of Fowler loop and frequent
short stretches of Bozeman rides particularly along pedestrian paths, extensive tree coverage and consequent persistent shade
provided cooler surface conditions than adjacent full-sun regions. Close inspections of Figure 1 clearly demonstrate shaded
regions of Fowler and Bozeman routes, as do temperature-time plots of Figs. 14 and spatial data of Fig. 15. These data show
that persistent shade leads to persistent surface cooling (including in winter) but that, in absence of shading or due to changes
815 in exposure that result in removal of shade, surface temperatures quickly revert to 'normal' for that ride at that time of day.
Intermittent shading, as from a road-side tree at early or late sun angles, presents a stiffer challenge but one still easily
resolved in these data. Figure 19 demonstrates CW (standard) followed by - minutes later - CCW Fowler loop rides: the
impact of one set of road-side trees shows very clearly in on the first southbound pass along the west lane but has no impact
a few minutes later as I rode back along the eastern lane. Both rides occurred around 1500 local time. (The Google Earth
820 image, conveying roughly the same sun angle, tends to reinforce measurements).

Figures D1 a-c demonstrate similar data gathered a few weeks later (27 July 2022) on (first) a northbound Bozeman ride
followed (roughly two hours later) by a southbound return ride. Panel 'a' shows the identical spot presented in Fig. 19: west-
side trees along south 3rd. In this early case (0700 start, 0900 return) neither initial northbound nor later southbound rides
showed any shading impact by west-side trees. Panel 'b' shows exit from (northbound) then return entry onto (southbound)
825 one of Bozeman's much-used pedestrian paths. Later southbound image demonstrated stronger surface heating in sun-
exposed areas plus stronger surface cooling in tree shaded areas: more-intense solar insolation provoked both more heating
and sharper shading/cooling. Panel 'c' demonstrates a similar effect. Sensors in early northbound passage showed modest to
slight impacts of exposure or shading while same sensors recorded, during later southbound passage, stronger surface
heating in exposed areas and stronger surface cooling in shaded areas.



830

835

840

Figure D1: Data from a northbound (0700) Bozeman ride followed by a southbound return ride a few hours later (after 0900), using identical temperature scales northbound and southbound, both on morning of 27 July 2022. (a) Data from early northbound ride (right track in east lane) followed less than 3 hours later by return (0930 local time) southbound ride (left track in west lane). Identical location as in Fig. 19. At these hours, with solar illumination from the east, neither ride shows any shade impact of trees on western roadside. (Google Earth image from Fig. 19, used again as background, recorded under late day conditions tends to confuse this early-in-the-day pattern). (b) Same day, same routes, showing data from northbound track (slightly mis-aligned) then southbound return track as I crossed from (rode into) pervious shaded graveled path via short paved (impermeable) access onto (from) standard Bozeman city streets. In this figure, later ride shows both sharper surface warming in sun-exposed spots and sharper surface cooling in tree shadows; rising morning sun tends to heat exposed surfaces while trees shade cooler surfaces. (c) Same day, same routes, showing data from south 3rd, along eastern tree-lined stretch. Early northbound (0700) track (right track along east lane) shows minor distinctions between shaded and un-shaded stretches. Later southbound return trip (left track along west lane) shows more surface heating in exposed areas plus stronger surface cooling in shaded stretches. Data from QGIS analysis include toggled layers of background imagery.



845 **Appendix E: Light measurements and NDVI calculations**

Intercomparisons of light data involve wavelengths, energy, exposures, units, etc.; not an easy task in ‘fixed location cases’, perhaps more difficult if one wants to validate bicycle systems involving inexpensive sensors moving between full sun and deep shade. Here I evaluate three components: a VEMML6030 light sensor on a bicycle, an identical VEMML6030 sensor mounted next to and parallel to roof panels, and roof-mounted photovoltaic panels measuring photovoltaic power in watts.

850 Figure 7 proves excellent correlations between roof-top panels and an adjacent roof-top VEMML6030 (the former recording power generation data in watts every 15 minutes while the latter records insolation in lux from 10 measurements averaged and transmitted every 5 minutes). Clouds should impose similar impacts on roof-top panels and roof-top light sensor, at least over longer (hourly, diel) time spans. Figures 12, B1 and B2 prove efficacy of comparing time-resolved bicycle light maxima to daily power-based insolation patterns; those intercomparisons prove effective and appropriate. Because of visible

855 differences in terrain and cloud cover, however, I did not compare local light (from photovoltaic panels or from roof-top VEMML6030 sensors) to 25-km distant NWS-generated light data. What about VEMML6030 sensors on a bicycle, gathering data at faster than 1 Hz at distances within 10 km of photovoltaic panels? With bicycle rides, at least for Fowler loop, complete within ~45 minutes, one might get at most four power data points from photovoltaic panels reporting every 15 minutes; not useful to extrapolate from ~4000 bicycle data points to 4 roof-panel data points. Roof-mounted VEMML6030

860 sensors, recording at ~30 seconds while reporting at five minutes repeat frequency, offer a useful validation bridge: even as bicycle sensors move in and out of local shade or experience, during a ride, changes in cloud cover, users will develop confidence in comparisons of like-for-like sensors (e.g., Figs. 7, 12, B1&2 compared to any seasonally-appropriate sensor data image). Users will quickly, as this user has, learn to identify and trust light changes, seasonal and direction-dependent rider shading (generally recorded in ride notes), and differing visible, UV and near-IR patterns related to rider-shading

865 versus, for example, clouds. This combination of slower power-based photovoltaic data with faster VEMML6030-based adjacent roof-top data with very fast (> 1 Hz) bicycle data can prove useful!

Pavement albedo (ratio of incoming to reflected light) might represent a determining factor in other environments (e.g., Pomerantz et al. 2000) but sensors used here provided unique valid records of both insolation and surface heating. Users can, if desired, calculate albedos by assuming spectral shapes normalized to AS7263 ‘red’ data, but actual measurements prove

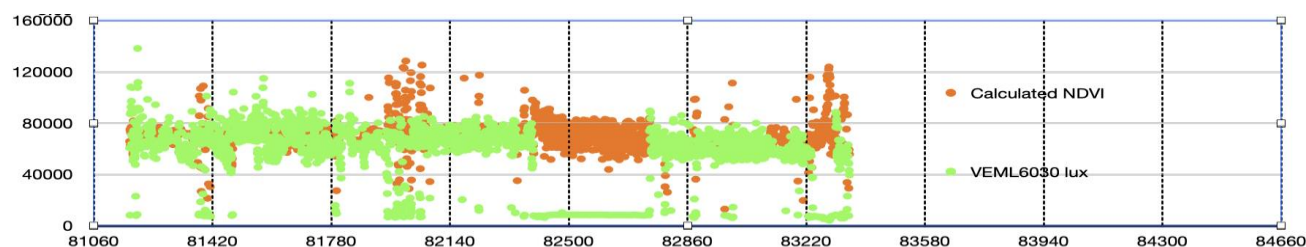
870 that, for these environments under these measurement conditions, air temperatures did not respond to underlying surface warming or cooling. Albedo changes, small in any case, proved irrelevant? Even under maximum surface heating conditions encountered within large cities, maximal plausible changes in albedo played only small (< 0.60 C) roles in surface-driven urban heat island effects (Pomerantz et al. 2000); their observations, weak as well as statistically non-determinant, neither explain nor contradict these measurements. Does solar insolation warm surfaces? Yes, definitively (see Fig. 18), but other

875 factors also pertain (data spread in Fig. 18). Should users therefore assume durable heat island influences? Not from these data as presented. We require more-careful, more-thorough assessments to account for or predict urban heating effects.

This configuration of sensors on this particular bicycle did not result in ideal locations for visible (VEMML6030, see Figs. 2 and 3) or UV light sensors (VEMML6075, again Figs. 2 and 3). At some seasons and times of day, upward-looking light sensors fell into shade of rider’s body or of bicycle handlebars or cables. These shaded directions and periods (often recorded



880 in notes accompanying each ride, see Appendix A) emerged distinctly in recorded light (Vis and UV) data (see for example Fig. E1).



885 **Figure E1: Data from Fowler loop ride on 2022-08-09, demonstrating cyclist-induced shading of light sensors on eastbound legs. Top: Garmin heading data; note (as always) two stretches of eastbound (90 degree) directions. Lower panel: light data (VEML6030, green dots) plus calculated NDVI (orange dots). VEML6030 data show sharp distinct diminutions (to very low lux) during two eastbound stretches starting around 82400 and 83200 seconds (approximately 1700 and 1710 local times). Light levels measured by VEML6030 remained approximately 60000 lux before and after periods of cyclist shading**

Moments or stretches of rider-induced shading of light sensors, easily distinguished from tree-induced or cloud-induced shading (clouds induce a more gradual transition with ‘softer’ edges), did not affect air or surface temperatures. For replication of rider-shading of light sensors, users can look at starting or ending loops (for example, in Fig. E2). There users will often note distinct directional influences on VEML6030 data, recorded accurately as bike changes of direction occurred much slower than VEML6030 response times. Note also (e.g., in Fig. 16) absence of corresponding direction- or speed-dependent impacts on surface or air temperatures.



895 **Figure E2: Data from Fowler loop ride on 2022-10-04, demonstrating cyclist-induced shading of light sensors during start and end loops. This image displays same tracks as in Fig. 16 (albeit with Google Earth background) but with VEML6030 lux data. For both start and end loops, light data showed greater values in northbound directions (upper right part of image) than in eastbound (lower left) directions.**

NDVI producers or users will know standard ranges of NDVI products: +1.0 to -1.0. NDVI calculations used here came from ratios of 680 nm and 860 nm data from AS7263, according to widely-accepted formula: $860 \text{ nm} - 680 \text{ nm} / \text{sum of } 680 \text{ nm plus } 860 \text{ nm}$. This author does not propose to open voluminous NDVI literature and interpretations; I only want to offer,



based on characterizations of surface temperatures, the possibility of applying local high-resolution but inexpensive data to larger NDVI applications and of interpreting satellite-based NDVI records based on bicycle-based surface data.

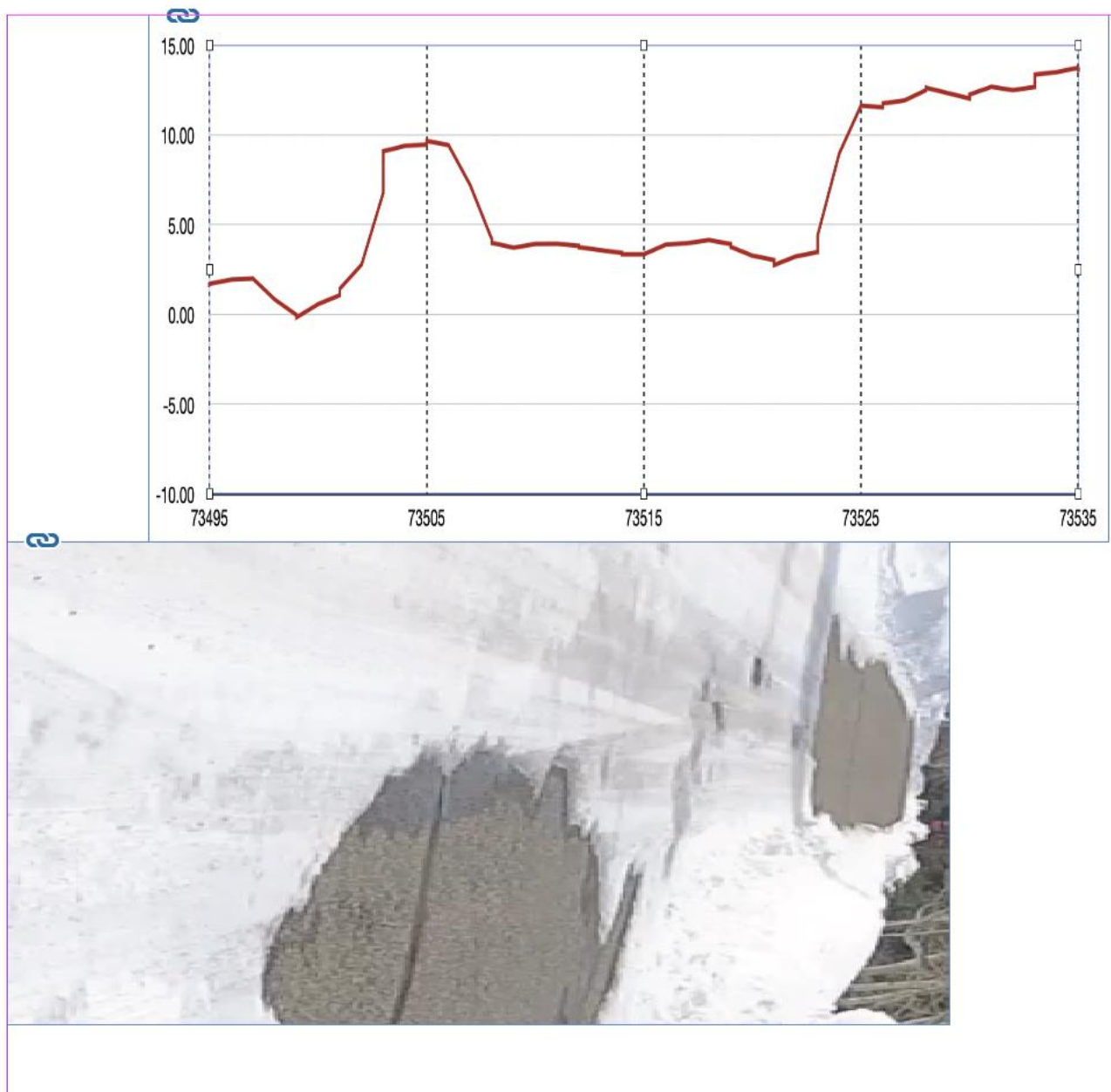
Appendix F: Winter conditions on impervious surfaces

905 Figure F1 demonstrates the considerable range of snow and ice covers of impervious surfaces available in this data set. Each of these conditions (packed snow versus vehicle-tracked ice) imposed different thermal and visible signatures.



910 **Figure F1: Data from Jade walk on 2023-03-09. Left image shows typical packed snow surfaces, after modest snow plowing. Right image shows vehicle packed ice, with vehicle wheel tracks clearly visible.**

Figure F2 demonstrates (imperfectly) how pavement temperatures differ between bare (end of cleared drive in near view), snow-covered, and (in the distance) bare surfaces. Pavement surface temperature differences from air temperatures varied in this case from near 0oC (air temperatures remained steady at +5oC throughout this record) over near-view snow to +10oC over cleared drive to greater than 10oC on solar-warmed pavements. A demonstration video
915 (<https://youtu.be/nMjBFbXxNWU>) combines drone plus bicycle-based videos with overlaid T_{sfc} and T_{air} data to provide users a better sense of extensive snow cover interspersed with spots of cleared or melted pavements, plus clear impacts of shade, for this particular Jade Street walk.



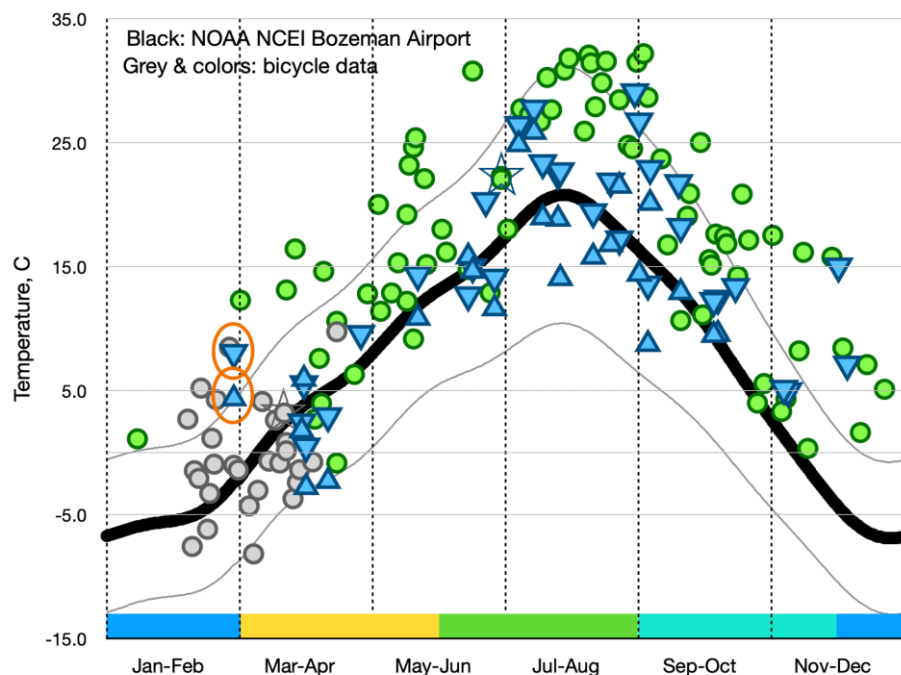
920 **Figure F2: Surface temperatures (top panel) superimposed over static photo of snow then shaded snow followed by bare (end-of-drive) surfaces, followed again by ice-covered then shaded then bare surfaces. Surface temperatures clearly respond to changes in surface coverage. Demonstration video shows this case in much better detail.**



Appendix G: Longer-term stability (durability) of sensors

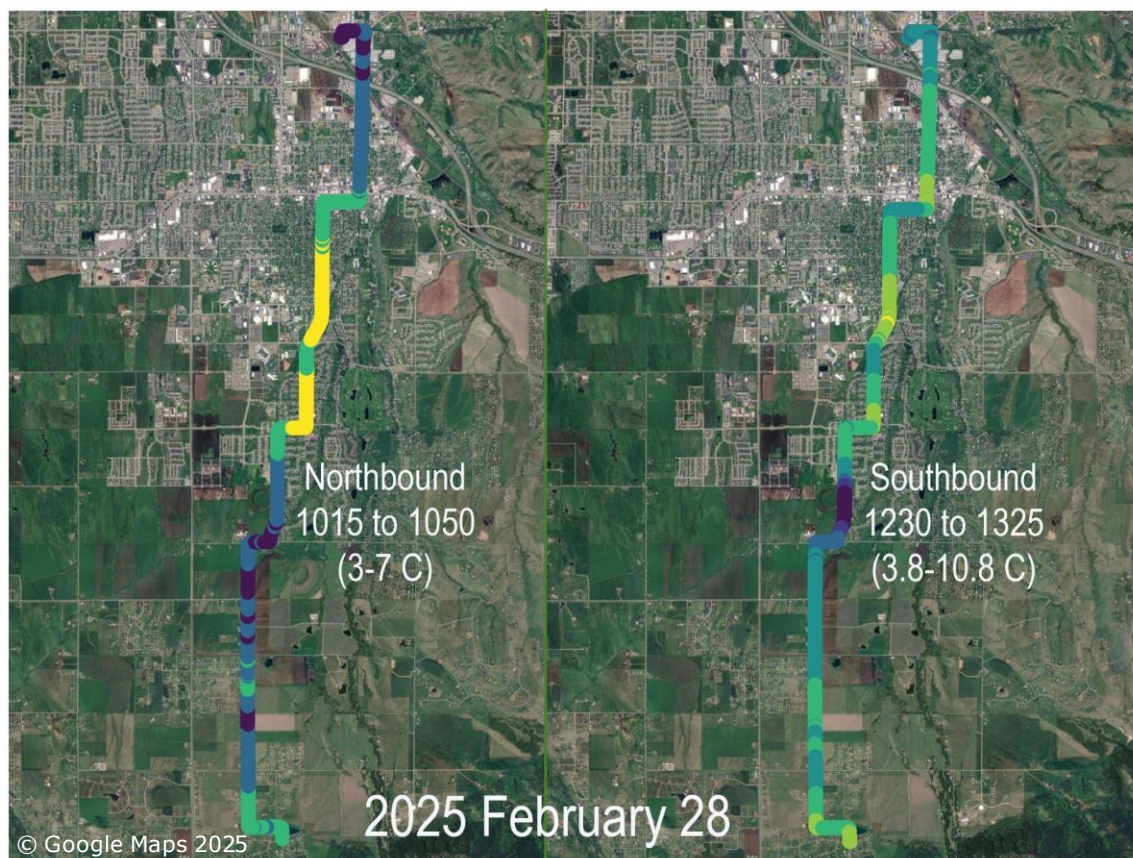
925 A bicycle ride on 28 February 2025, 16 months after ‘final’ (October 2023) data described here, proves long term durability
of these sensors. I used same bike, same box, same sensors, and same power, on a ride to and from north Bozeman; I
930 recorded this data under appropriate file label (2025-02-28 Bozeman) but never included 2025 data in any analysis above.
These data reveal several interesting features, ripe for confirmation or refutation by subsequent bicycle riders.

1. Fundamental durability of these sensors. They record data nearly identical to that gathered many months (16
930 months) earlier. Primarily for reasons of repeatability (out-and-back rides along an ‘unfamiliar’ route, relatively
warm daily conditions, etc.), I did not include 2025 data in any analysis above. But 2025 data along commonly-
measured stretches of south 3rd Avenue would easily fit with earlier 2022-2023 data (e.g., Fig. G1).
2. The difficulty - in and around Bozeman - of ensuring adequate coverage of multiple features. One needs, even
in this small city, a fleet of bicycles making repeated coordinated survey-type measurements.
- 935 3. The complexity of winter-time measurements, with piles of melting snow beside and impinging on many E-W
and N-S ‘city’ streets plus grit/gravel spread around corners and along busier streets.
4. Evidence for ‘interesting’ thermal features (e.g. ‘cold’ air temperatures along open stretches of south 3rd
Avenue with apparently warmer air temperatures along ‘town’ streets) not related, at least in obvious manner,
to surface temperatures (Fig. G2).



940

Figure G1: Data exactly as in Fig. 11 (above) with additions (circled in orange) of northbound (upward triangle) and southbound (downward triangle) data from 28 February 2025. Within normal variations due to weather, sunlight, etc., 2025 data fit perfectly with all prior data.



945 **Figure G2:** Air temperature (TMP117) image from QGIS, northbound and southbound rides to/from Bozeman, 28-02-2025. Google Earth backgrounds in both cases; note different (time-dependent) air temperature ranges. Mean data from stretches along south 3rd Avenue reported in Fig. G1.